A holistic thermoeconomic assessment of small-scale, distributed solar organic Rankine cycle (ORC) systems: Comprehensive comparison of configurations, component and working fluid selection

Yaxiong Wang[1,2], Jian Song[2], Maria Anna Chatzopoulou[2], Nixon Sunny[2,3], Michael C. Simpson[2], Jiangfeng Wang[1,*], Christos N. Markides[2,*]

[1] *Institute of Turbomachinery, Xi'an Jiaotong University, Xi'an, China*

[2] *Clean Energy Processes (CEP) Laboratory, Department of Chemical Engineering, Imperial College London, London SW7 2AZ, UK*

[3] *Centre for Environmental Policy, Imperial College London, Exhibition Road, London, SW7 2AZ, UK*

** Corresponding authors. E-mail addresses: jfwang@xjtu.edu.cn, c.markides@imperial.ac.uk*

N.B.: This is the ACCEPTED version of this article. The final, published version of the article can be found at: https://doi.org/10.1016/j.enconman.2021.114618

Abstract

In this paper, results from comprehensive thermoeconomic assessments of small-scale solar organic Rankine cycle (ORC) systems are presented based on weather data in London, UK, which is taken as representative of a temperate climate with modest temperature changes, mild winters and moderate summers. The assessments consider a range of: (i) solar collector types (flat-plate, evacuated-tube, and evacuated flat-plate collectors); (ii) power cycle configurations (basic/recuperative, partial/full evaporating, and subcritical/transcritical cycles); (iii) expander types (scroll, screw, and piston) and designs; and (iv) a set of suitable working fluids. All possible solar-ORC system designs are optimised by considering simultaneously key parameters in the solar field and in the power cycle in order to obtain the highest electricity generation, from which the best-performing systems are identified. A representative number of selected designs are then subjected to detailed, annual simulations considering the systems' operation, explicitly considering off-design performance under actual varying weather conditions. The results indicate that, among all investigated designs, solar-ORC systems based on the subcritical recuperative ORC (SRORC), evacuated flat-plate collectors (EFPCs), a piston expander, and isobutane as the working fluid outperforms all the other system designs on thermodynamic performance, whilst having the highest annual electricity generation of 1,100 kW ħ/year (73 kW ħ/year/m^2) and an overall thermal efficiency of 5.5%. This system also leads to the best economic performance with a levelised cost of energy (LCOE) of ~1 $/kW ħ. Apart from the specific weather data used for these detailed system simulations, this study also proceeds to consider a wider range of climates associated with other global regions by varying the solar resource available to the system. Interestingly, it is found that the optimal solar-ORC system design remains unchanged for different conditions, however, the LCOE can drop below 0.35 $/kW ħ and payback times can be shorter than 16 years in high solar-resource regions, even in the absence of incentives that would otherwise lead to even better economic performance. This work complements previous efforts in the literature by considering the full design and operational features of solar-ORC systems, thereby providing valuable guidance for selecting appropriate cycle configurations, components, working fluids and other characteristics and, for the first time, presents a comprehensive comparison of such systems in small-scale applications.

Keywords:
organic Rankine cycle, renewable energy, solar energy, thermoeconomic optimisation, working fluid

Nomenclature

Abbreviations

a_1, a_2	solar collector coefficients, W/(m^2·K), W/(m^2·K^2)
A	area, m^2
Bo	boiling number
c_1, c_2	heat transfer correction factors for evaporation process
c_3, c_4	pressure correction factors for evaporation process
c_5, c_6	heat transfer correction factors for condensation process
c_7, c_8	pressure correction factors for condensation process
c_{el}	electricity price, $/(kW ħ)
C	cost, $
f_p, f_0, f_1	correction factor for pressure
G	solar irradiance, W/m^2
G_p	mass velocity, kg/(s·m^2)
h	specific enthalpy, J/kg
h_{lg}	specific enthalpy of vaporisation, J/kg
i_d	discount rate
i_F	inflation rate
L	length, m
$\dot{m}$	mass flow rate, kg/s
M	mass, kg
N	plant lifetime, year
Nu	Nusselt number
P	pressure, Pa or bar
Pr	Prandtl number
$\dot{q}$	heat flux density, W/m^2
$\dot{Q}$	heat flow rate/thermal load, W
Re	Reynolds number
S_p	passage cross-sectional area, m^2
t	time, s
T	temperature, K or ℃
u	velocity, m/s
U	overall heat transfer coefficient, W/(m^2·K)
v	kinematic viscosity, m^2/s
$\dot{V}$	volumetric flow rate, m^3/s
V	volume, m^3
V_r	volume ratio

$\dot{W}$	power, W
W	energy, J or kW ħ
x	fluid quality
z	corrugation depth, m

Greek symbols

α	heat transfer coefficient, W/(m^2·K)
β	corrugations angle, rad
η	efficiency
η_0	optical efficiency
λ	thermal conductivity, W/(m·K)
μ	dynamic viscosity, Pa s
ρ	density, kg/m^3

Subscripts

1-4, 2', 4'	state points
a	ambient
ann	annual
cond	condenser
d	design condition
eq	equivalent
evap	evaporator
exp	expander
I	investment
in	inlet
l	liquid
loss	loss
net	net power output
out	outlet
p	passage
pump	pump
recup	recuperator
sc	solar collector
screw	screw expander
sh	superheat degree
th	thermal
tk	tank
u	useful

v	vapour
wf	working fluid

Acronyms

CHP	combined heat and power
EFPC	evacuated flat-plate collector
ETC	evacuated-tube collector
FPC	flat-plate collector
GWP	global warming potential
HTF	heat transfer fluid
LCOE	levelised cost of energy
ORC	organic Rankine cycle
PBT	payback time
PCM	phase change material
PEC	partial evaporation cycle
SNORC	subcritical non-recuperative organic Rankine cycle
SRORC	subcritical recuperative organic Rankine cycle
TES	thermal energy storage
TLC	trilateral cycle
TNORC	transcritical non-recuperative organic Rankine cycle
TRORC	transcritical recuperative organic Rankine cycle

1. Introduction

As a renewable, sustainable and abundant resource, solar energy can play a leading role as a primary vector in energy systems. With suitable technologies it can be harnessed to generate and to deliver electricity, heat and/or cooling with low environmental impact in a wide range of applications. Relevant studies have focused on advances in photovoltaic (PV) [1–3] and concentrated solar power (CSP) systems [4–6] and also more recently, but less so, on hybrid PV-thermal (PVT) systems [7–9], all of which have attracted attention as options for (primarily) generating electricity from sunlight. The role of PV is the most well-understood, and CSP is considered particularly suitable for larger-scale power systems as it benefits more than PV from both economies of scale as well as performance benefits at larger scales; it also promises added advantages in co-/poly-generation applications and/or applications where storage is of interest as it can make use of low-cost thermal energy storage (TES).

Recently, non-concentrated solar-based technologies based on thermodynamic power cycles have emerged as a promising alternative to PV for small-scale solar power systems, especially in domestic and building applications where energy storage is beneficial to technical and economic system operation and co-generation is of interest. Freeman et al. [10] presented an assessment of a domestic combined heating and power (CHP) system based on an organic Rankine cycle (ORC) utilising solar energy as the energy input. Their results showed that an annually averaged power output just under 90 W could be obtained from a 15 m^2 area, i.e., ~6 W/m^2 or ~50 kW ħ/year/m^2, along with a hot water coverage of close to 90% of a typical family's need in the UK. The authors expanded their original study to include organic working fluid selection and parametric optimisation in Ref. [11], where results showed that using a single-stage system configuration with R245ca yielded the highest annual electricity generation of ~60 kW ħ/year/m^2, and that an improved dual-collector configuration had an annual power production that was higher by 12%. The same authors also studied a range of energy storage (in fact, TES) solutions for solar-ORC systems by comparing different combinations of collectors and phase change materials (PCMs) [12]. Their findings suggested that, in the UK climate, storage amounting to ~400 L of an inorganic hydrated-salt PCM was required to shift the generation of a 1 kW-scale power output solar-ORC system driven by a 15 m^2 solar array of evacuated flat-plate collectors away from the core daylight hours to coincide with the evening peak in electricity demand.

In related work, Ramos et al. [13] optimised solar-ORC systems for domestic buildings by considering two types of solar collector and seven working fluids. The optimisation results showed that, for a 60 m^2 flat-plate solar collector array in south European regions (average irradiance 600 W/m^2), the average power of such systems was 460 W when using R245fa as the working fluid, and that for evacuated-tube collectors the average power increased significantly to 1700 W (±20 W) with R1233zd as the working fluid. Sonsaree et al. [14] also analysed the performance of small-scale ORC power systems exploiting three different types of collector, i.e., flat-plate collectors (FPCs), evacuated-tube collectors (ETCs) and compound parabolic concentrators (CPCs), with the proposed systems achieving a levelised cost of energy (LCOE) of 0.67-0.84 $/kW ħ. Turning their attention to the influence of the working fluid properties on the performance of a small-scale solar-ORC system, Helvaci et al. [15] found

a highest system thermal efficiency of 9.6% with 1-butene as the working fluid. Furthermore, Wang et al. [16] presented results from a study of power systems driven by solar energy in the domestic context, where the performance of systems employing both conventional and pumpless ORC systems were compared, with results showing that pumpless systems had a higher net power output by 3.3%. Beyond fist-law (i.e., energy-based) analyses, Roumpedakis et al. [17] performed combined exergetic and economic analyses of a solar-ORC system, and concluded that a maximum exergy efficiency of 6.2% was achievable with R245fa as the working fluid and with evacuated-tube collectors.

Basic subcritical ORCs were generally considered in the aforementioned investigations, however, other ORC architectures, such as trilateral ORCs (TLCs), partial evaporation ORCs (PECs), as well as transcritical ORCs, may offer performance benefits and warrant further investigation. Yari et al. [18] conducted thermodynamic and thermoeconomic comparisons of TLC and ORC systems exploiting a low-grade heat source at 120 ℃. Their results showed that a TLC system with n-butane exhibited the highest power output, while an ORC system with n-butane yielded the lowest investment cost. Li et al. [19] also performed comparative analyses of a basic ORC system and a TLC system at different evaporation temperatures, and concluded that the TLC system achieved a maximum net power output which was 37% higher than that of the ORC system for a case study with an evaporation temperature of 152 ℃. Zhou et al. [20] analysed the performance of a PEC system and found that employing optimal operating parameters for such a system can lead to a higher net power output by close to 25% compared to a conventional subcritical ORC system. An in-depth thermodynamic comparison of PEC and subcritical ORC systems was also performed by Lecompte et al. [21], who showed a ~10% increase in the annual energy production by the PEC system relative to the ORC system. The same authors proceeded to compare transcritical ORC, subcritical ORC and PEC systems using an exergy approach in Ref. [22], with results indicating that the PEC system outperformed the other two by more than 20% in terms of exergy efficiency for low-temperature (~100 ℃) waste-heat recovery. Moreover, Zeynali et al. [23] investigated the performance of various solar-ORC configurations, and showed that recuperative ORC systems were associated with the highest net power output, and Oyewunmi et al. [24] optimised recuperative subcritical and transcritical ORC systems while employing more than 35 working fluids, with results demonstrating that transcritical ORC system may offer superior thermodynamic performance in some cases.

In addition to the ORC system architecture, the choice of components also impacts system performance. As a critical component, the selection of the expander and its corresponding efficiency have significant effects on the overall performance of ORC power systems. Volumetric expanders, such as screw [25], scroll [26] and piston [27] machines, are often preferable for small-scale ORC systems as they are tolerant of two-phase expansion and have low manufacturing and operational complexity. Dumont et al. [28] presented an experimental investigation of four common expander types in subcritical conditions, and reported highest measured efficiencies for scroll, screw, piston and roots expanders of 76%, 53%, 53%, and 48%, respectively. Similar work was done by Guillaume et al. [29], with five positive displacement expanders modelled based on experimental results and a semi-empirical methodology, illustrating the variation of the expander isentropic efficiency as a function

of the pressure ratio across the component. For expanders experiencing two-phase expansion, a reduction in the isentropic efficiency was noted because of inadequate heat transfer between the liquid bulk and surface of the machine [30], and a similar drop in the isentropic efficiency was observed by Öhman et al. [31]. For supercritical expansion, limited literature is available and the maximum reported isentropic efficiencies of scroll, screw and piston expanders identified by the present authors in the literature are 45% [32], 56% [33] and 32% [34], respectively. It is important to note, when considering TLC, PEC and transcritical ORC systems that although these systems may offer different improved (in some cases) thermal match with the heat source, and therefore improved thermodynamic performance as indicated by theoretical studies, often these assume a fixed (common) expander isentropic efficiency for all system types, although it is known that this will vary; a deterioration in expander efficiency may negate any performance improvements and requires further investigation.

While the performance of various solar-ORC systems has been investigated and compared in a number of specific case studies, considering different cycle configurations and working fluids, less research has focused on whole-system optimisation of domestic solar-power systems from a more holistic and comprehensive perspective. This paper addresses this research gap by investigating the combined thermodynamic and economic performance of a wide range of domestic solar-ORC systems based on weather data in London, UK, which is taken as representative of a temperate climate with modest temperature changes, mild winters and moderate summers. A comprehensive optimisation problem considering six power cycle configurations (TLC, PEC, subcritical basic/recuperative ORC, transcritical basic/recuperative ORC), three collector types (flat-plate, evacuated-tube, and evacuated flat-plate collectors), three expander designs (scroll, screw, and piston), and sixteen working fluids is formulated, and used to obtain the optimal (maximum) annual electricity generation potential of these systems, along with key corresponding economic figures-of-merit (LCOE, payback time). Subsequently, off-design analysis is performed to screen the best-performing designs accounting for their performance under actual variable operating conditions. Furthermore, the solar conditions are extended to a wider range of climates to evaluate system performance in different global regions. To the best of the authors' knowledge, this study is the first to present a comprehensive comparison of a range of domestic-scale solar-ORC system variants and their thermoeconomic performance under a range of climates, within a unified modelling framework that promotes more confident comparisons between the systems.

2. Modelling and optimisation methods

A schematic diagram of the investigated solar-ORC systems is shown in **Figure 1**. The systems comprise two main sections, i.e., the solar field and power cycle. The solar-collection field covers an area of 15 m^2, which is both the average roof-space area available in UK homes for the installation of such system as used in the authors' previous work, as well as the size approximately required to provide power to a typical UK family, which has an average electrical power consumption of 1 kW [12]. The solar field absorbs heat from the sun, and the power cycle converts this into electricity. A two-tank configuration is applied to buffer the temporal variability in the solar irradiance. In the solar field, low-

temperature heat transfer fluid (HTF) is stored (accumulated) in a low-temperature tank (LT tank) and pumped from there through the collectors to be heated. Therminol VP-1 [35] is selected as the HTF. Similarly, high-temperature HTF from the collectors is stored in a high-temperature tank (HT tank). A bypass is installed between the solar field and the HT tank in case the HTF temperature does not reach the required storage temperature. In this case, the HTF is returned to the collectors for further heating. Six power-cycle configurations, or architectures, are investigated: (i) subcritical non-recuperative ORCs (SNORCs); (ii) subcritical recuperative ORCs (SRORCs); (iii) transcritical non-recuperative ORCs (TRORCs); (iv) transcritical recuperative ORCs (TRORCs); (v) TLCs; and (vi) PECs. The organic working fluid is pumped into the evaporator where it is heated by the HTF that flows from the HT tank. The high-temperature and high-pressure working fluid expands in the expander to generate power, and then enters the condenser where it is cooled by cooling water, completing the cycle. A recuperator (or, internal heat exchanger) can be incorporated into the power cycle for internal heat recovery from the expander outlet. The component models and economic models are presented in the following sections.

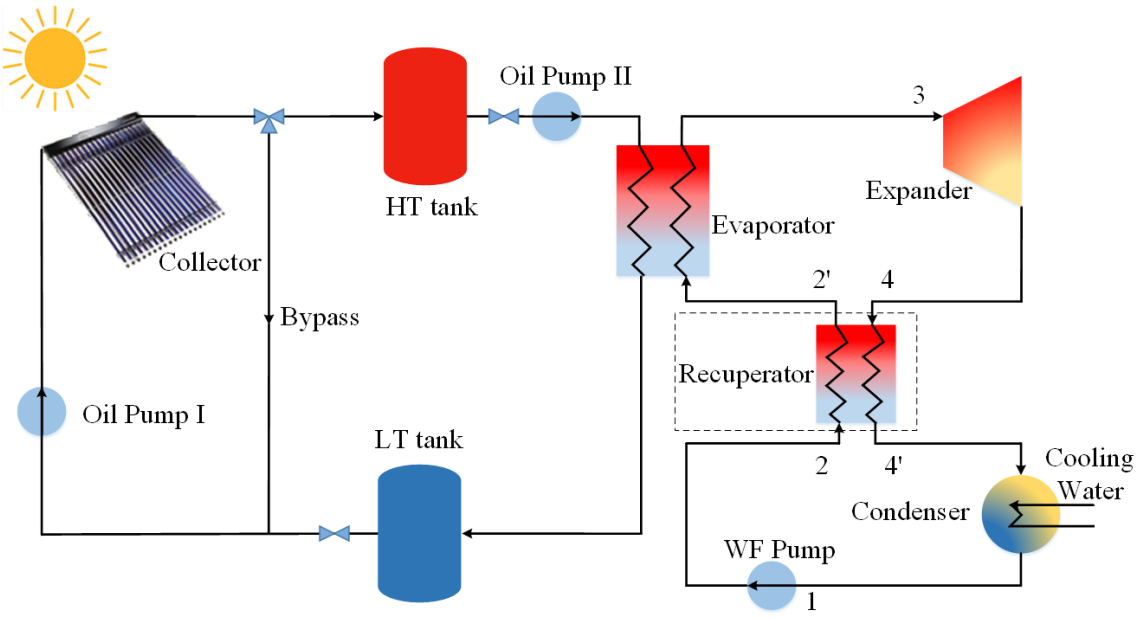

Figure 1. Schematic diagram of the solar-ORC systems considered in this work. The power cycle can vary, and it can be configured with or without a recuperator (internal heat exchanger).

2.1. Solar collectors

Three types of collectors are considered in this work: (i) flat-plate collectors (FPCs); (ii) evacuated-tube collectors (ETCs); and (iii) evacuated flat-plate collectors (EFPCs). Among the commercial solar collectors available on the market, PremiumPlus designed by Solarbayer [36], DF100 designed by ThermoMax [37] and MT-Power designed by TVP Solar [38], respectively, are selected, and their efficiency parameters are given in **Table 1**. The useful heat absorbed by the collector is determined by the total area of the solar collector, solar irradiance, and collector efficiency:

$$\dot{Q}_u = G A_{sc} \eta_{sc}, \quad (1)$$

where the collector efficiency η_{sc} is given by a classical parabolic equation:

$$\eta_{sc} = \eta_0 - \frac{a_1\left(T_{sc} - T_a\right)}{G} - \frac{a_2\left(T_{sc} - T_a\right)^2}{G}. \tag{2}$$

Table 1. Efficiency parameters of the three representative collector products considered in this work.

Product	**Type**	η_0	a_1	a_2
PremiumPlus [36]	FPC	0.78	3.68	0.007
Thermomax DF100 [37]	ETC	0.77	1.43	0.006
TVP MT-Power [38]	EFPC	0.76	0.51	0.007

2.2. Tanks

The HT tank and LT tank are modelled dynamically using the following equations. A non-stratified tank assumption is applied, such that the fluid (HTF) temperature inside the tank is uniform [39].

The mass conservation equation inside the tank can be written as:

$$\frac{dM_{tk}}{dt} = \dot{m}_{HTF,in} - \dot{m}_{HTF,out}. \tag{3}$$

The energy balance equation of the tank is expressed by:

$$M_{tk} c_p \frac{dT_{tk}}{dt} = \dot{Q}_{tk,in} - \dot{Q}_{tk,out} - \dot{Q}_{tk,loss}, \tag{4}$$

where T_{tk} is the HTF average temperature inside the hot tank.

The inlet heat, the outlet heat, and the heat loss can be calculated from:

$$\dot{Q}_{tk,in} = \dot{m}_{HTF,in} c_p \left(T_{HTF,in} - T_{tk}\right), \tag{5}$$

$$\dot{Q}_{tk,out} = \dot{m}_{HTF,out} c_p \left(T_{HTF,out} - T_{tk}\right), \tag{6}$$

$$\dot{Q}_{tk,loss} = U_{tk,a} A_{tk} \left(T_{tk} - T_a\right). \tag{7}$$

2.3. ORC power-cycle system

The thermodynamic models of the six investigated cycle configurations are listed in **Table 2**. Recuperative cycles represent subcritical recuperative ORC and transcritical recuperative ORC, while non-recuperative cycles include subcritical non-recuperative ORC, transcritical non-recuperative ORC, trilateral cycle and partial evaporation cycle.

Table 2. Thermodynamic models of ORC components and indicator definitions.

Component/indicator	**Recuperative cycles**	**Non-recuperative cycles**
Evaporator	$\dot{Q}_{evap} = \dot{m}\left(h_3 - h_{2'}\right)$	$\dot{Q}_{evap} = \dot{m}\left(h_3 - h_2\right)$
Condenser	$\dot{Q}_{cond} = \dot{m}\left(h_{4'} - h_1\right)$	$\dot{Q}_{cond} = \dot{m}\left(h_4 - h_1\right)$

Recuperator	$\dot{Q}_{\text{recup}} = \dot{m}\left(h_{2'} - h_2\right) = \dot{m}\left(h_4 - h_{4'}\right)$	N/A
Pump, Expander	$\dot{W}_{\text{pump}} = \dot{m}\left(h_{2\text{s}} - h_1\right)/\eta_{\text{pump}}$, $\dot{W}_{\text{exp}} = \dot{m}\left(h_3 - h_{4\text{s}}\right)\eta_{\text{exp}}$	
Net power output	$\dot{W}_{\text{net}} = \dot{W}_{\text{exp}} - \dot{W}_{\text{pump}}$	
Thermal efficiency	$\eta_{\text{th}} = \dot{W}_{\text{net}} / \dot{Q}_{\text{evap}}$	

Plate heat exchangers are selected on account of their low cost and suitability for small-scale applications (such as in the present work). There is a great range of designs for plate heat exchangers on the market, depending on the application and the operating conditions. The plates can be corrugated to enhance heat transfer, and improve rigidity, but at the expense of higher pressure drops. The corrugations, and the narrow paths developed for the flow, result in higher HTCs and *U*-values, increasing the heat transfer rate per m^2 of heat transfer area. Consequently, plate heat exchangers are suitable for applications where the physical size of the system is a restriction, and they are selected for all the six power cycle configurations in this study. The calculations of heat transfer coefficients and pressure drops for both the HTF and the working fluid are given in Appendix A.

2.4. Expander

Positive displacement expanders are chosen as the expansion devices, as they are appropriate for small- to medium-scale power systems and can accommodate two-phase expansion is correctly designed and operated. Screw expander, scroll expander, and piston expander are the three most common types of positive displacement expander, and as such have been studied in many previous investigations (e.g., see Refs. [40,41]). Therefore, these types of expander are included in this study.

2.4.1. Screw expander

The correlation proposed by Astolfi et al. [42] is applied to calculate the screw expander efficiency at both design and off-design conditions. The correlation is derived using performance data of screw compressors available on the market [42]. The expander efficiency in design condition is given by:

$$\eta_{\text{d,screw}} = \text{c}\left[0.9403305 + 0.0293295\text{In}\left(\dot{V}_{\text{out}}\right) - 0.0266298 V_{\text{r}}\right], \tag{8}$$

$$c = 1, \text{ for } V_{\text{r}} \le 7; \; c = 1 - 0.264\text{In}\left(V_{\text{r}}/7\right), \text{ for } V_{\text{r}} > 7 . \tag{9}$$

where $\dot{V}_{\text{out}}$ is the working fluid volumetric flow at the outlet of the expander, and V_{r} is the volume ratio of the working fluid flowing through the screw expander, which is defined as the ratio of the specific volume of the working fluid at the outlet of the expander to that at the inlet.

At off-design conditions, the expander efficiency can be calculated from:

$$\eta_{\text{off,screw}} = \eta_{\text{off,screw}}\left[-0.0323\left(\frac{V_{\text{r,off}}}{V_{\text{r}}}\right)^4 + 0.288\left(\frac{V_{\text{r,off}}}{V_{\text{r}}}\right)^3 - 0.8995\left(\frac{V_{\text{r,off}}}{V_{\text{r}}}\right)^2 + 1.006\left(\frac{V_{\text{r,off}}}{V_{\text{r}}}\right) + 0.6056\right]. \tag{10}$$

2.4.2. Scroll expander

Scroll expanders have been investigated in many experimental studies to obtain their performance maps [43,44]. The isentropic efficiency of the scroll expander is determined utilising the experimental data from Lemort et al. [44], where the authors conducted a test on a small-scale (~1 kW) scroll expander. The measured scroll expander efficiency and its fitted correlation are shown in **Figure 2**.

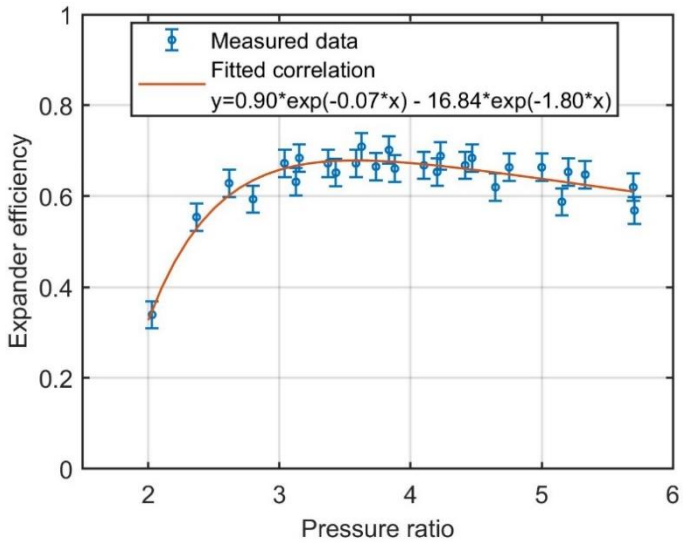

Figure 2. Measured scroll expander efficiency in Ref. [44] and the fitted correlation used in this study. The power out of the expander is 0-3 kW, and the inlet pressure of the expander ranges from 670 kPa to 1600 kPa, which are in-line with the investigated cases in this paper.

2.4.3. Piston expander

An in-house MATLAB code was used to model the piston expander and to obtain overall efficiency maps, as in previous studies by the authors; see, for example, Refs. [45–48]. Full details can be found in Ref. [45,46], where the development of a lumped-mass model accounting for various losses was described, including pressure losses, heat losses, and mass leakage. Separate piston expander efficiency maps for all selected working fluids were generated using the model. As an example, **Figure 3** shows the performance map of the piston expander with isobutane as the working fluid.

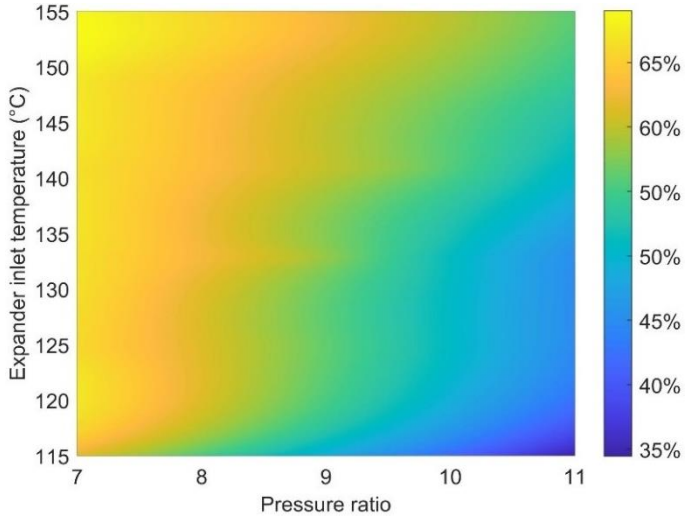

Figure 3. Piston expander performance map (isentropic efficiency) with isobutane as the working fluid.

2.5. Economic analysis

Empirical cost correlations are used to estimate the total investment cost of the solar-ORC systems. The correlations deployed and the associated variables of all components are summarised in **Table 3**. It should be noted that economic models for different expanders are rare in the literature. Alshammari et al. [49] compared the costs of various expander types and gave detailed cost correlations, which were closely aligned with market prices. For example, the market price of a 1 kW-scale scroll expander with a built-in pressure ratio around 3 should be of the order of several thousand dollars; the price predicted by Alshammari et al. [49] was $2,200. Consequently, the model presented by Alshammari et al. [49] is used in this study, in which the cost of expanders were correlated as a function of the power output (in kW).

Table 3. Component cost models used in the present study.

Component	Associated variables	Cost, $
FPC	Collector area A, m^2	150 A [13]
ETC	Collector area A, m^2	162 A [12]
EFPC	Collector area A, m^2	216 A [12]
Scroll expander	Expander power output $\dot{W}$, kW	2200 $\dot{W}$ [49]
Screw expander	Expander power output $\dot{W}$, kW	5800 $\dot{W}$ [49]
Piston expander	Expander power output $\dot{W}$, kW	2400 $\dot{W}$ [49]
Plate heat exchanger	Heat exchanger area A, m^2	205 + 335 A [50]
Pump	Pump power consumption $\dot{W}$, kW	972 $(\dot{W}/0.3)^{0.25}$ [50]

The economic analysis of the solar-ORC systems is based on two main indicators, specifically, the levelised cost of energy (LCOE) and payback time (PBT). The LCOE is a widely used indicator that is used to evaluate and compare the economic performance of solar power systems [9,14,51,52]. It is a measure of the average cost (per unit of electrical energy, in kW·h) generated by a power system over its lifetime. It is defined as the total discounted cost divided by the total discounted electricity amount over the system's lifetime, and it can be expressed as:

$$\mathrm{LCOE}=\left[C_{\mathrm{I}}+\sum_{n=1}^{N}\frac{C_{\mathrm{ann}}\left(1+i_{\mathrm{F}}\right)^{n-1}}{\left(1+i_{\mathrm{d}}\right)^{n}}\right]\Big/\sum_{n=1}^{N}\frac{W_{\mathrm{ann}}}{\left(1+i_{\mathrm{d}}\right)^{n}}. \tag{11}$$

where the inflation rate i_{F} is taken as 2.5% [8], the discount rate i_{d} is set to 5% [9], the system lifetime N is assumed to be 20 years [39], and W_{ann} is the annual electricity generation.

The payback time can be calculated from the common expression [9]:

$$\mathrm{PBT}=\mathrm{In}\left[\frac{C_{\mathrm{I}}\left(i_{\mathrm{F}}-i_{\mathrm{d}}\right)}{W_{\mathrm{ann}}c_{\mathrm{el}}}+1\right]\Big/\mathrm{In}\left(\frac{1+i_{\mathrm{F}}}{1+i_{\mathrm{d}}}\right). \tag{12}$$

where the electricity purchase price c_{el} is taken as 0.19 $/kW h, both corresponding to the UK from Ref. [52].

No further incentives are considered, such that the availability of such benefits can lead to an economic performance that is even better than what is indicated here, e.g., lower LCOE and shorter PBT.

2.6. Operational strategies and assumptions

The tanks are designed to have a storage capacity equivalent to 5 hours of operation time, which means the solar-ORC system can generate power for up to 5 hours after sundown (when the solar irradiance is insufficient); this discharge time is a typical value that has been applied elsewhere in the literature, e.g., in a real solar power plant in Ottana, Italy [39]. The HTF flow rate is adjusted by controlling Oil Pump I (see **Figure 1**), to keep the HTF temperature at the solar-field outlet equal to the HT-tank storage temperature. When the irradiance is low and HTF outlet temperature is lower than the HT-tank storage temperature, the bypass valve in the solar field opens and the HTF is sent back to the collectors to be heated until it reaches the required set point, which is a decision variable to be optimised in this study.

Furthermore, although the investigation is in its latter stage generalised in a geographically agnostic manner (**Section 3.5**), London is chosen as an initial investigated location (**Sections 3.1-3.4**) in this study, for which hourly solar irradiance and ambient temperature data acquired from the climate database in EnergyPlus [53]. The key assumptions made in this study are listed below:

(1) The total collector area is 15 m^2, which is the typical available roof area in a UK household [10–12].

(2) The pump efficiency is assumed to be 0.7, which has also been used in similar studies [20,54].

(3) In the analyses in **Sections 3.1** and **3.2**, where the expander type is not specified, the expander efficiency is 0.7, which is a typical efficiency found in the literature [15,48]. In **Section 3.3**, i.e., in the system optimisation process, a range of expander efficiencies are considered, as shown in **Table 5**. It is noted that only the solar-array area is fixed (15 m^2) in this study, while expander size is not fixed and adjusted for different working fluids and cycle configurations.

(4) All components except for the tanks are assumed to operate in quasi-steady-state conditions.

(5) The minimum pinch point temperature difference in the heat exchangers is assumed to be 5 ℃.

(6) Heat losses are only considered from the tank to the ambient in the annual operation analysis (i.e., not for the design operating conditions and sizing).

(7) The power consumption by all system auxiliaries, e.g., HTF circulation pumps, ORC cooling water pump, is neglected in accordance with Refs. [11,55,56]; we have checked this assumption and confirmed that this amounts to <1% and ~2% of the total generated power in this work.

Finally, all fluid properties are obtained from the NIST REFPROP database [57].

2.7. Optimisation method

The operating parameters of the domestic solar-ORC systems under investigation are optimised so as to obtain the highest annual electricity generation, which is reported here in units of kW ⋅h per year. The optimiser considers six types of power-cycle configurations, including TLCs, PECs, SNORCs, SRORCs, TNORCs and TRORCs, and three types of expanders, including scroll, screw and piston expanders. Furthermore, two types of solar collectors, namely ETCs and EFPCs are considered; FPCs were excluded due to their relatively poor performance, as shown in **Section 3.1**. Sixteen organic working fluids are included, which are listed in **Table 4** – ten fluids with a low global warming potential (GWP) and good thermodynamic properties [40] are selected for systems based on TLCs, PECs, SNORCs and SRORCs, and six fluids with a low critical temperature for systems based on TNORC sand TRORCs, as suggested by Kosmadakis et al. [32].

Table 4. Critical temperatures and GWP of selected working fluids for: (a) TLC-, PEC-, SNORC- and SRORC-based systems as per the work of Bao and Zhao [40]; and (b) TNORC- and TRORC-based systems as per Kosmadakis et al. [32].

(a) Fluid	**R1234yf**	**R1234ze**	**R152a**	**Isobutane**	**Butane**
Critical temperature (℃)	95	109	112	135	152
GWP	1	1	124	1	1
Fluid	R245fa	R1233zd	R245ca	Isopentane	Pentane
Critical temperature (℃)	153	164	174	187	196
GWP	1030	1	693	1	1

(b) Fluid	**R125**	**R143a**	**R32**	**R404a**	**R410a**	**R407c**
Critical temperature (℃)	66	72	78	72	73	86
GWP	3500	4470	675	3922	2088	1774

The solar field and the power cycle are simultaneously optimised to achieve the maximum annual electricity generation of the overall system, based on the objective function:

$$f = \text{maxmise}\frac{\{W_{\text{ann}}\}}{\vec{X}}. \tag{13}$$

and the decision variables for each cycle configuration as well as the constrains are given below.

For TLCs:

$$\vec{X} = [T_{\text{LT,tank}}, T_{\text{HT,tank}}, T_{\text{cond}}, T_{\text{evap}}]. \tag{14}$$

For PECs:

$$\vec{X} = [T_{\text{LT,tank}}, T_{\text{HT,tank}}, T_{\text{cond}}, T_{\text{evap}}, x_{\text{evap,out}}]. \tag{15}$$

For SNORCs and SRORCs:

$$\vec{X} = [T_{\text{LT,tank}}, T_{\text{HT,tank}}, T_{\text{cond}}, T_{\text{evap}}, T_{\text{sh}}]. \tag{16}$$

For TNORCs and TRORCs:

$$\vec{X} = [T_{\text{LT,tank}}, T_{\text{HT,tank}}, T_{\text{cond}}, T_{\text{evap}}, P_{\text{evap}}]. \tag{17}$$

Several constrains are imposed as part of the optimisation process, which are listed below:

(1) The pressure ratio of the scroll expander is within the range of 1.5-5.5 [44,58–60], the pressure ratio of the screw expander is within the range of 2-8 [61–64], and the pressure ratio of the piston expander is within the range of 4-11 [28,29,65].

(2) The expander efficiencies for solar-ORC systems with different cycles and expander types are reported in **Table 5** based on typical values found in literature.

(3) The minimum continuous operation period of the solar-ORC systems is 1 hour, which is selected to ensure that the system is not subjected to multiple stop/start routines which would reduce

the lifetime of the mechanical components. Based on this control strategy, Oil Pump II is switched on to pump the HTF to the ORC system evaporator when there is sufficient heat input to drive the power cycle for more than 1 hour, and the power cycles are assumed to be operated only in full load in the optimisation process, at design conditions.

(4) For subcritical cycles, $T_{evap} < 0.98\ T_{critical}$.

(5) For transcritical cycles, $T_{evap} > T_{critical} + 5$ ℃.

(6) For the fully evaporated ORC configurations, two-phase flow should not occur in the expander.

(7) For partial evaporated cycles, $0.05 < x_{evap,out} < 0.95$.

As shown in **Table 5**, in the performance predictions of the SNORC- and SRORC-based systems, the expander efficiencies are based on the models presented in **Section 2.4**. For TLC and PEC-based systems, the expander efficiencies are assumed to be 5% (in absolute value terms) lower to account for an efficiency reduction/performance deterioration in two-phase expansion as reported in Refs. [30,31]. For systems based on transcritical cycles, models to calculate the expander efficiency are lacking, so experimental data from Refs. [32–34] are used.

Table 5. Expander efficiency design set-point used in the optimisation process.

	TLC, PEC	**SNORC, SRORC**	**TNORC, TRORC**
Scroll expander	60%	65%	45% [32]
Screw expander	55%	60%	56% [33]
Piston expander	60%	65%	32% [34]

3. Results and discussion

In **Section 3.1**, representative results are shown first from a sensitivity analysis conducted to examine the impact of the tank storage temperatures on the thermal performance of the solar field, for different types of collector and a selected power-cycle configuration (i.e., SNORC) with R245fa. This is followed, in **Sections 3.2** and **3.3**, by design optimisation of six different power cycles/system types, components and working fluids, for given tank storage temperatures and a fixed expander efficiency that depends on the expender technology. In **Section 3.4**, results are shown from performance studies in which optimal system designs are identified while considering off-design operation. All results in **Sections 3.1** to **3.4** are optimisation solutions for maximum power generation on an annual basis, with time-varying operation using annual hourly solar irradiance data in London, UK. Finally, in **Section 3.5**, the thermoeconomic performance of solar-ORC systems is investigated in multi-regional climatic conditions, which are varied parametrically in steady-state (not time-varying) simulations using two parameters to describe the solar resource, namely the average solar irradiance and solar sunshine hours.

3.1. Sensitivity analysis

In this section, we first evaluate the influence of the tank storage temperatures on the solar array thermal performance on an annual basis, using annual hourly solar irradiance data in London as input, for all three collector types, i.e., FPCs, ETCs, and EFPCs. In this analysis, the HTF flow rate through the solar field is adjusted according to the solar irradiance and the LT-tank temperature in order to heat the HTF to the temperature of the HT tank. If the irradiance is not enough to heat the HTF outlet temperature to the HT tank conditions, a bypass is used; details are given in **Section 2.6**. The ORC system is only operated (switched on) when there is enough HTF in the hot tank (being discharged) to allow the ORC system to operate continuously for at least 1 hour. We assume no heat losses and the ORC system is always operated at a full (100%) load condition with periodic start-up/shut-downs in response to the varying thermal-energy availability from the storage tanks. Since the capacity/size of the storage tanks is set such that the ORC system can operate for up to 5 hours (**Section 2.6**), and the power cycles are operated only at full load, the tank size affects the design value of the HTF flow rate to the power cycle. A smaller tank is cheaper, but also has a reduced annual storage capacity.

Of interest, therefore, in this section are the optimal HTF flow rates to the ORC system from the storage tanks which allow the solar field to attain the maximum annual thermal-energy gain (**Figures 5** and **6)**, and the ORC system to generate the maximum annual electricity generation. To this end, we select a SNORC system with R245fa as the working fluid and evaluate the influence of the tank storage temperatures on the performance of this specific power cycle (**Figure 7**). A fixed (technology agnostic) expander isentropic efficiency of 0.7 is considered, and cycle parameters, i.e., evaporation/condensation temperatures and superheating degree, are optimised to achieve the maximum electrical power generation for each set of tank storage temperatures within specified ranges: from 40 ℃ to 80 ℃ for the LT tank, and from 100 ℃ to 180 ℃ for the HT tank. Finally, we evaluate the influence of the two storage temperatures on the electricity generation potential of the combined solar-ORC system (still a SNORC system with R245fa and an expander isentropic efficiency of 0.7) on an annual basis (**Figure 8**).

When EFPCs are used, taken here as an example collector type, it can be seen from **Figure 4** that, for given tank storage temperatures, there exists a minimum HTF flow rate delivered to the ORC evaporator between the two storage tanks (see also **Figure 1**) that is associated with the best annual thermal-energy gain and collector thermal efficiency; these points are marked by an asterisk in the figure, and are regarded as the optimal flow rates for this collector type and conditions. Any flow rate higher than this does not lead to any further gains in either the annual thermal-energy gain by the tanks or in the collector thermal efficiency. Optimal HTF flow rates for all investigated tank storage temperatures obtained from figures similar to **Figure 4** but for the full range of both tank storage temperatures are summarised in **Figure 5** when using EFPCs. From **Figure 5**, it can be seen that the optimal flow rate ranges from 0.025 kg/s to 0.1 kg/s, increasing at higher LT-tank storage temperatures and lower HT-tank storage temperatures, i.e., as the temperature difference across the solar collector field reduces.

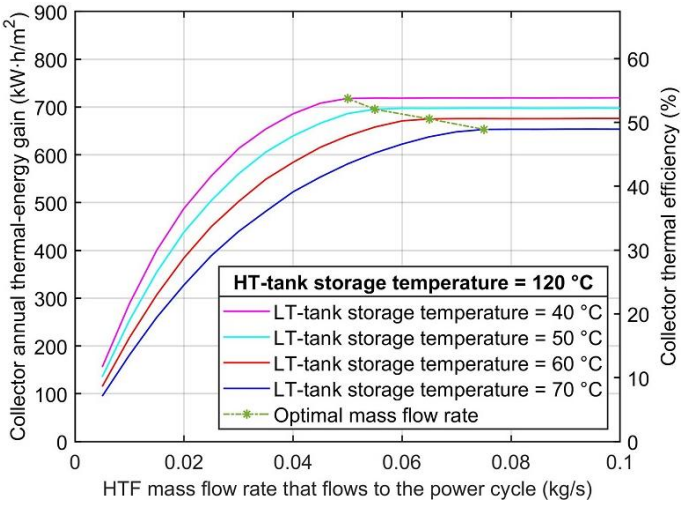

Figure 4. Annual thermal-energy gain and thermal efficiency of EFPC solar fields for different HTF flow rates to the ORC evaporator, a HT-tank temperature of 120 ℃ and different LT-tank temperatures. Results were obtained for a solar array area of 15 m^2 and annual hourly weather data in London, UK.

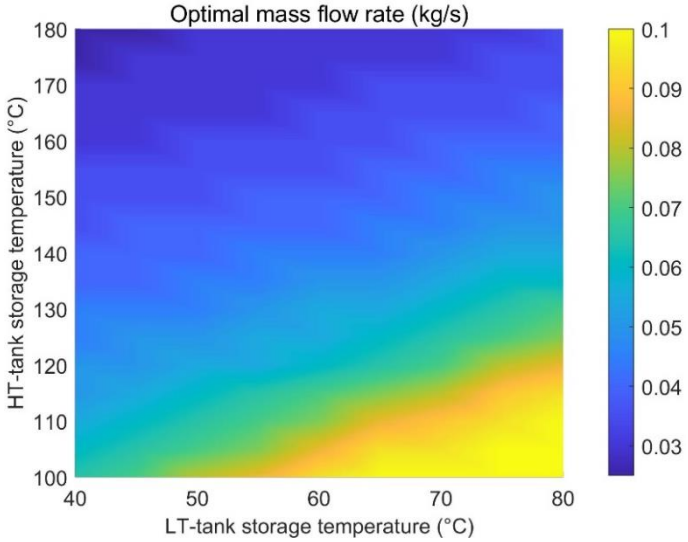

Figure 5. Optimal HTF flow rates to the ORC evaporator in EFPC solar fields. With the optimal HTF flow rate, the maximum thermal-energy gain of the solar field with specific tank storage temperatures could be achieved with the lowest possible tank costs. Results were obtained for a solar array area of 15 m^2 and annual hourly weather data in London, UK.

A similar procedure can be applied to calculate the optimal HTF flow rates for other collector types, namely in this work, FPCs and ETCs. **Figure 6** shows the annual thermal-energy gain and thermal efficiency of all three investigated collector types, with respect to the LT- and HT-tank storage temperatures. The annual thermal-energy gain and thermal efficiency increase at lower tank storage temperatures, thanks to the reduced losses from the solar collectors when these are operated at temperatures closer to the ambient. The collectors have the highest thermal efficiency when the HT- and LT-tank temperatures are at their lowest set limits (100 ℃ and 40 ℃), at which operating point the efficiencies of the FPCs, ETCs and EFPCs attain values of 32%, 51%, and 57%, respectively. Based on a total solar-array area of 15 m^2, the annual thermal-energy gains when employing FPCs, ETCs and EFPCs corresponding to their highest thermal efficiencies are 23.2 GJ, 37.0 GJ, and 41.1GJ.

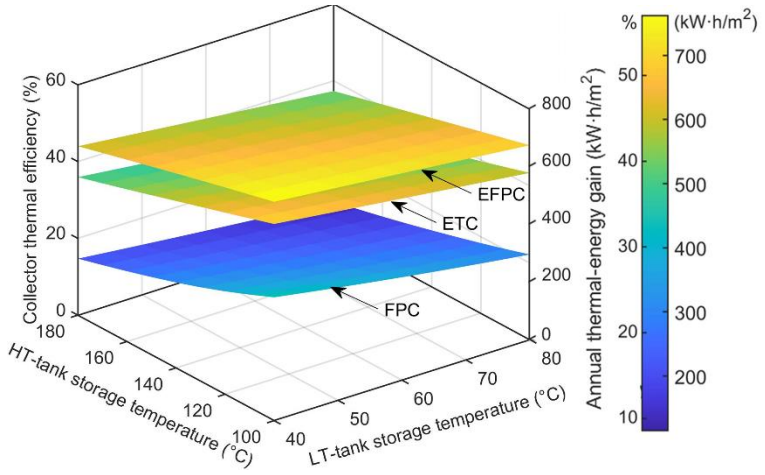

Figure 6. Variation of collector thermal efficiency and annual thermal-energy gain with the tank storage temperatures for the three types of collectors considered in this work (FPCs, ETCs, EFTCs). Results were obtained for a solar array area of 15 m^2 and annual hourly weather data in London, UK.

For given tank storage temperatures, the annual electricity generated by the system is a function of both the annual thermal-energy gain in the solar field and the thermal efficiency of the power cycle, which coincides with the highest annual electricity output from the wider system. Taking the SNORC with R245fa as an example system, and for a solar field with EFPCs, **Figure 7** shows that the thermal efficiency of the power cycle increases with both tank temperatures, as expected. Interestingly, however, the thermal efficiency achievable by SNORC systems reaches a maximum of ~9%, with no further gains at even higher storage temperatures. This limit arises due to the fact that the evaporating temperature in the power cycle is constrained by the critical temperature of the organic fluid (153 ℃ for R245fa). Of note is also the considerable variability (factor of 2) of the thermal efficiency.

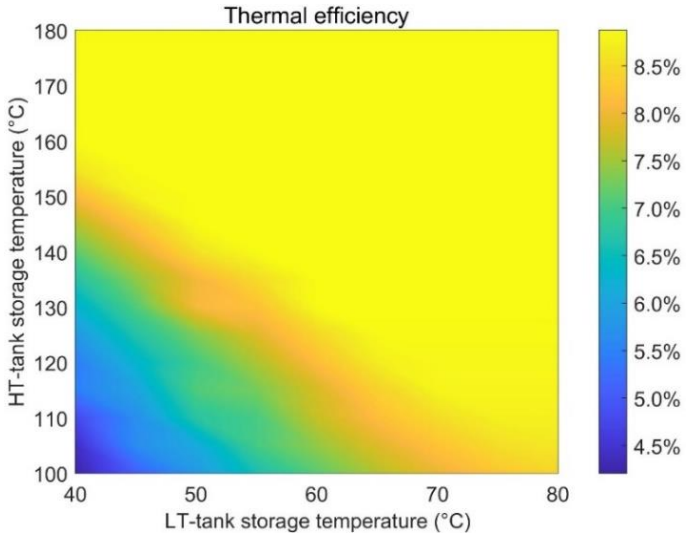

Figure 7. Thermal efficiency of the ORC power cycle for different (steady-state) tank storage temperatures, with EFPCs, a SNORC as the power cycle configuration, and R245fa as the working fluid.

Combining the annual thermal-energy gain potential in the solar field and the thermal efficiency of the power cycle, **Figure 8** shows the annual electricity generation by the wider system, which reaches a maximum of ~800 kW h at a corresponding cycle thermal efficiency of ~4% when the HT- and LT-tank temperatures reach 160 ℃ and 40 ℃, respectively. It is interesting to note that this performance by the solar-ORC system is associated with the lowest LT-tank temperature and a high, but not the highest, HT-tank temperature. Importantly, 800 kW h of electricity is enough to cover ~25% of the electricity usage of a typical UK household, which was reported to be 3,100 kW h in 2017 in Ref. [66].

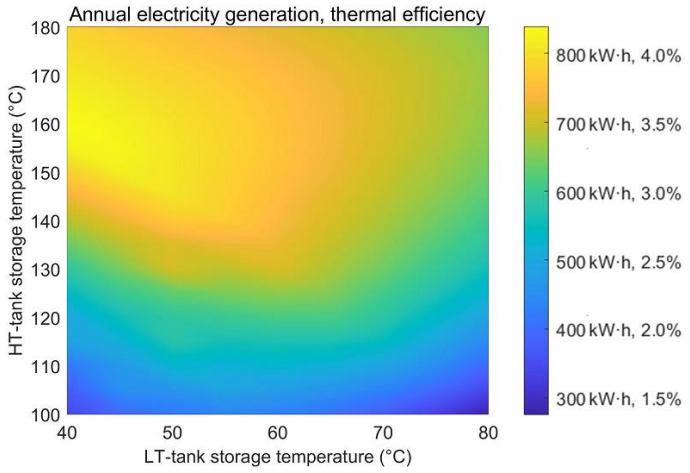

Figure 8. Annual electricity generation and thermal efficiency of the overall solar-ORC system for different tank storage temperatures, with EFPCs, a SNORC as the power cycle configuration, and R245fa as the working fluid. The thermal efficiency is obtained by dividing the annual electricity generation by the annual solar irradiation over the collector area, i.e., ~20,000 kW h over 15 m^2. Results were obtained for a solar-array area of 15 m^2 and annual hourly weather data in London, UK.

The results and associated discussion above indicate that there is a trade-off between the solar-field efficiency and the ORC power-cycle efficiency, since the maximum ORC thermal efficiency (**Figure 7**) is achieved at the highest tank storage temperatures, and therefore also, highest solar field temperatures, that result in the lowest collector efficiencies (**Figure 6**). This observation is noteworthy and highlights the fact that the tank storage temperature is important in its ability to affect the performance of both the solar field and the power cycle, and should be optimised to improve overall system performance. The results also reveal that ETCs and EFPCs outperform FPCs by considerable margins (>60% and >80%, respectively). On this basis, and considering their similar costs to those of ETCs (see **Table 3**), FPCs are excluded from further investigation (for the present application).

3.2. Preliminary comparison of configurations

In this section, we select one collector type (EFPC) and one working fluid (R1234yf) in order to explore the influence of the tank storage (i.e., heat-source) temperatures on the performance of optimal (evaporation/condensation temperatures, superheating degree) solar-ORC systems based on

all six configurations of interest on an annual basis in terms of maximum annual power generation.

To this end, a comparative study was first performed of the thermal-matching characteristics of the TLC, PEC, SNORC, SRORC, TNORC and TRORC system configurations with the heat source, which in this work is the HTF fluid flow delivered to the ORC system. **Figure 9** shows examples of optimised cycles for the particular case when the HT- and LT-tank storage temperatures are set to 150 ℃ and 40 ℃, respectively. For these specified tank storage temperatures and a fixed (technology agnostic) expander isentropic efficiency of 0.7 for all configurations, the transcritical ORC system has the best thermal-matching characteristics, followed by the two subcritical ORCs, PEC and TLC.

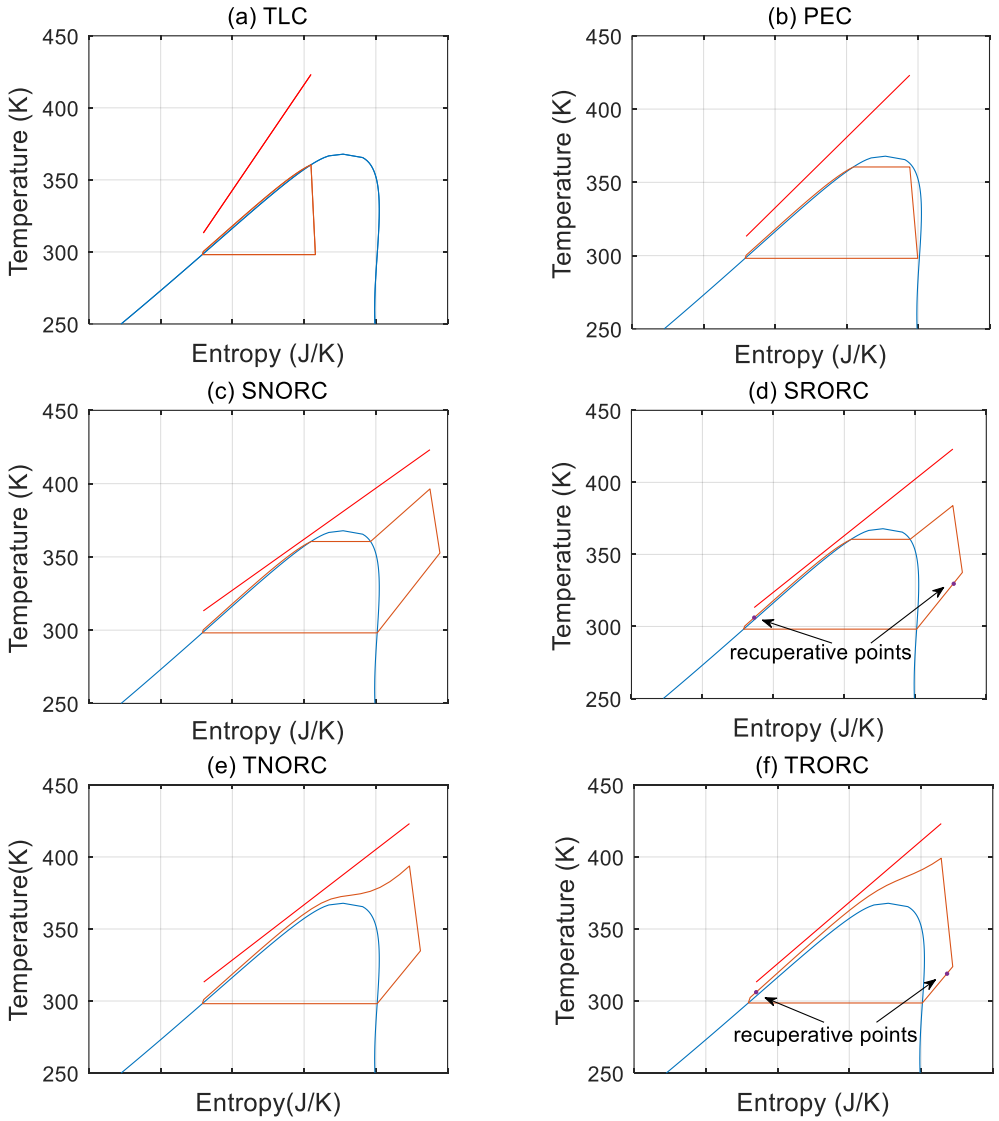

Figure 9. *T-s* diagrams corresponding to: (a) TLC, (b) PEC, (c) SNORC, (d) SRORC, (e) TNORC; and (f) TRORC system configurations with R1234yf as the working fluid, HT-tank and LT-tank storage temperatures set to 150 ℃ and 40 ℃, respectively, and a constant expander isentropic efficiency of 0.7. All cycle parameters are optimised to achieve the highest thermal efficiency.

Importantly, **Figure 10** quantifies the maximum annual electricity generation that can be generated by all the six cycle configurations when the HT-tank and the LT-tank temperatures are relaxed from

their aforementioned values. For this working fluids, the highest annual electricity generation (~1170 kW h) and thermal efficiency (~6%) are achieved by the TRORC system configuration, which is favoured when the HT-tank storage temperature is higher than 118 ℃. At lower HT-tank storage temperatures, the SRORC system configuration is preferable when the LT-tank storage temperature is above 58 ℃, and the PEC is favoured when the LT-tank temperatures is below 58 ℃. It should be noted that, in practice, existing options of expansion devices for expanding fluids in the two-phase and near-critical regions are relatively immature, especially in the applications of interest here. As such, there is a need for comprehensive, whole-system optimisation that accounts for any performance variability in this, amongst other, components, when identifying optimal system architectures/configurations.

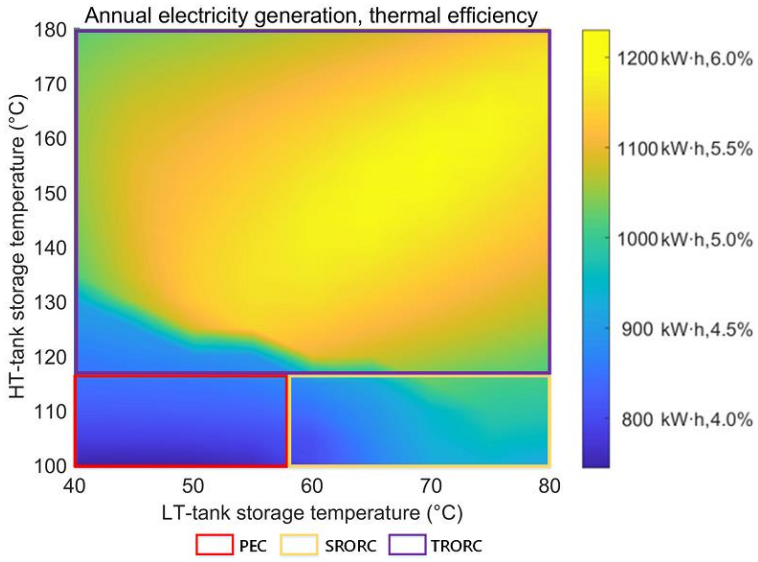

Figure 10. Performance map of maximum annual electricity generation and thermal efficiency for different tank storage temperatures, showing preferable cycle/system configurations with R1234yf as the working fluid and a constant expander isentropic efficiency of 0.7. The thermal efficiency is obtained by dividing the annual electricity generation by the annual solar irradiation over the collector area, i.e., ~20,000 kW h over a solar-array area of 15 m^2. Results were obtained for annual hourly weather data in London, UK.

3.3. System optimisation at design conditions

In this section, results are shown from comprehensive optimisation of all six cycle configurations, two collector types (ETCs and EFPCs, since FPCs were excluded from further consideration in **Section 3.1**), three expander designs, and a range of organic fluids conducted to maximise annual electricity generation. The decision variables from **Section 2.7**, including tank storage temperatures and cycle parameters, were simultaneously optimised to maximise the annual electricity generation based on annual hourly solar irradiance data in London. In these simulations, different expander isentropic efficiencies corresponding to the type and application are considered, no heat losses are assumed, the ORC system is always operated at a full (100%) load condition when operational, and switched off otherwise, with frequent start-up/shut-downs. Results are presented concerning the annual power generation and corresponding LCOEs of all designs (for maximum annual power generation).

3.3.1. Cycle configuration comparison

As shown in **Figure 11-16**, solar power systems based on SRORCs outperform the other five configurations in terms of electrical output due to: (i) their higher expander efficiency compared to TLCs, PECs and transcritical ORCs; and (ii) the thermodynamic performance benefit afforded by the recuperator compared to the SNORC configuration. SRORC systems generate the highest annual electrical output of 1,080 kW ħ (with a corresponding thermal efficiency of 5.4%) among the six cycle configurations, followed by the SNORC with 999 kW ħ, PEC with 924 kW ħ, TRORC with 893 kW ħ, TLC with 834 kW ħ, and TNORC with 726 kW ħ. For subcritical, partially evaporated cycles, PEC systems improve upon the thermoeconomic performance of TLCs for all the considered fluids, collectors, and expanders. Furthermore, the PEC has a comparable performance with the SRORC when using isopentane or pentane as the working fluid. For subcritical ORCs, the SRORC is better than the SNORC for most of fluids except for isopentane and pentane, and a substantial improvement is noted for fluids with low critical temperature such as R1234yf and R1233ze. For transcritical ORCs, an enhancement of more than 10% in the electricity generation is achieved by adding a recuperator. For all the cycles, a high annual electricity generation always corresponds to a low LCOE. The SRORC has the lowest LCOE (as low as ~1 $/kW ħ) among the six cycles. The LCOE of PEC and the SNORC is marginally (0.1-0.3 $/kW ħ) greater than that of the SRORC, while the TLC and the transcritical ORCs both have high LCOEs ranging from 1.3-3.5 $/kW ħ.

3.3.2. Collector comparison

For all the investigated combinations, systems using EFPCs are more cost-effective than ETCs as they can generate more electricity annually (50-200 kW ħ more than ETCs) at lower LCOE (~0.2 $/kW ħ lower than ETCs) values. This is because: (i) the EFPCs have a higher thermal efficiency than the ETCs, translating into a thermodynamic improvement of 15-20%; and (ii) the EFPCs are only marginally more expensive than the ETCs, which would cause a total cost increase of ~8%.

3.3.3. Expander comparison

For subcritical cycles as shown in **Figure 11-14**, the piston expander is the best-performing expander for almost all the working fluids, in terms of annual electricity generation, owing to its high efficiency and wide range of feasible pressure ratios. The scroll expander has a high efficiency at low pressure-ratios, while the screw expander has a lower efficiency and a higher pressure ratio than the scroll expander. The LCOE of solar power systems is highly affected by the expander cost. Systems with screw expanders have the highest LCOE because of its high cost, while systems with the other two types of expanders have comparative LCOE in most cases because of the similar expander costs.

For the transcritical cycles in **Figure 15** and **16**, the screw expander is the preferred expansion technology thanks to its relatively high efficiency. It also leads to a higher annual electricity generation (520-900 kW ħ, 150-200 kW ħ higher than a scroll expander) and a similar LCOE (1.7-2.2 $/kW ħ) relative to scroll expanders, due to its higher unit cost. Piston expanders are less desirable in this case due to their lower annual electricity generation (250-400 kW ħ) and higher LCOE (2.2-3.4 $/kW ħ).

3.3.4. Working fluid comparison

For the TLC shown in **Figure 11**, the best-performing fluids are isobutene, butane, and isopentane. Other fluids with high critical temperatures, such as R245fa, R1233zd, R245ca, and pentane, also have a good performance, while those with a lower critical temperature (R1233yf, R1234ze, and R152a) yields lower annual electricity and higher LCOE. For the PEC shown in **Figure 12**, the fluids with critical temperature in the range of 135-187 ℃ have similar thermodynamic and economic performance, while the other fluids (R1233yf, R1234ze, R152a, and pentane) have worse performance. For the SNORC shown in **Figure 13**, R152a, isobutane, and butane are the best-performing working fluids, R1234yf and pentane yield the worst performance. For the SRORC as shown in **Figure 14**, the performance of fluids with low critical temperatures are greatly improved by adding the recuperator. For TNORC- and TRORC-based systems as shown in **Figure 15** and **16**, R404a is the most preferable fluid, followed by R410a, R32, R143a, R407c, and R125.

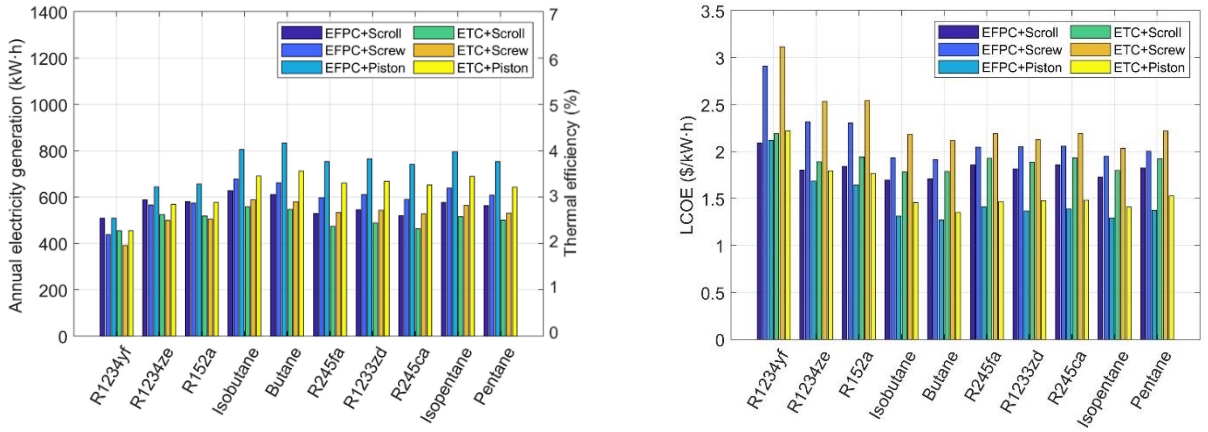

(a) (b)

Figure 11. (a) Annual electricity generation; and (b) corresponding LCOE for solar-ORC systems based on TLCs. Ten investigated fluids are displayed in order of increasing critical temperature and cycle parameters optimised to achieve maximum annual electricity generation. Results were obtained for a solar-array area of 15 m^2 and annual hourly weather data in London, UK.

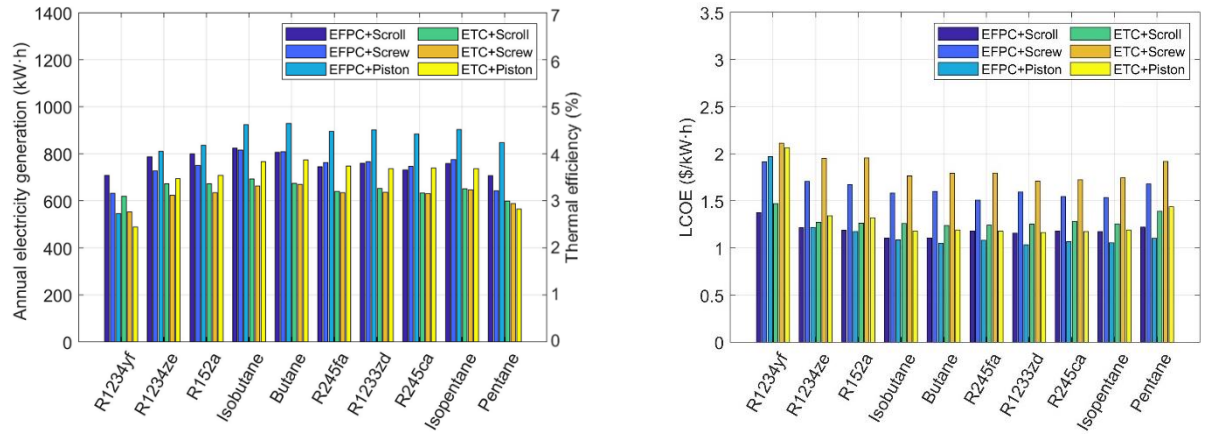

(a) (b)

Figure 12. (a) Annual electricity generation; and (b) corresponding LCOE for solar-ORC systems based on PECs. Ten investigated fluids are displayed in order of increasing critical temperature and cycle parameters optimised to achieve maximum annual electricity generation. Results were obtained for a solar-array area of 15 m^2 and annual hourly weather data in London, UK.

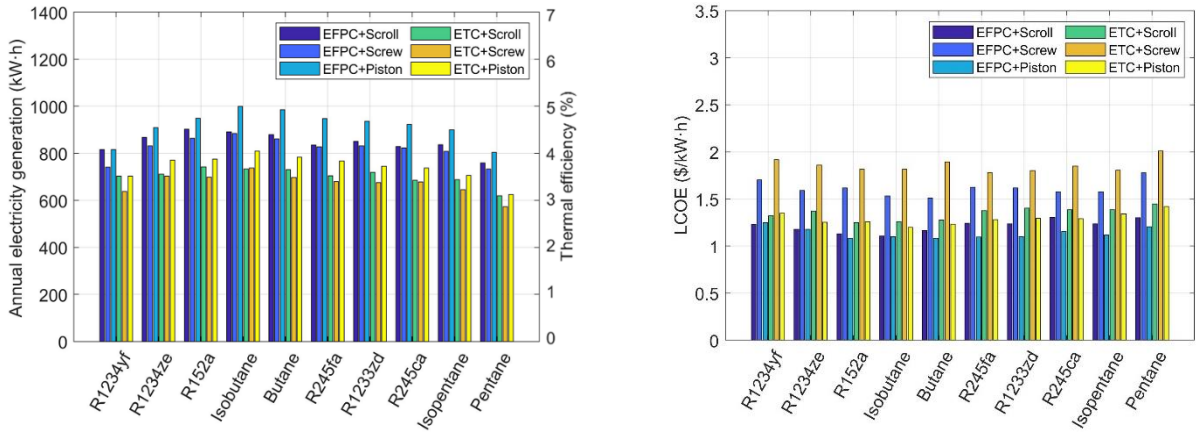

(a) (b)

Figure 13. (a) Annual electricity generation; and (b) corresponding LCOE for solar-ORC systems based on SNORCs. Ten investigated fluids are displayed in order of increasing critical temperature and cycle parameters optimised to achieve maximum annual electricity generation. Results were obtained for a solar-array area of 15 m^2 and annual hourly weather data in London, UK.

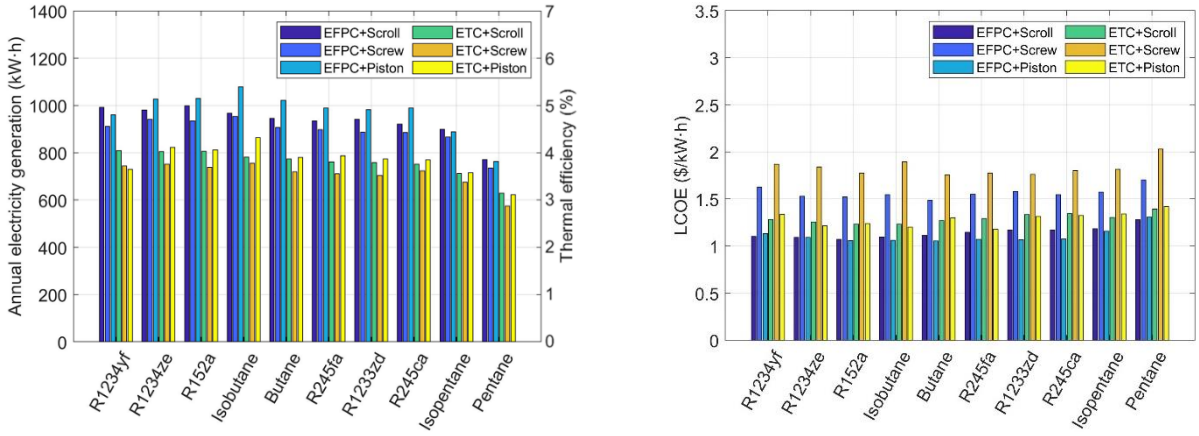

(a) (b)

Figure 14. (a) Annual electricity generation; and (b) corresponding LCOE for solar-ORC systems based on SRORCs. Ten investigated fluids are displayed in order of increasing critical temperature and cycle parameters optimised to achieve maximum annual electricity generation. Results were obtained for a solar-array area of 15 m^2 and annual hourly weather data in London, UK.

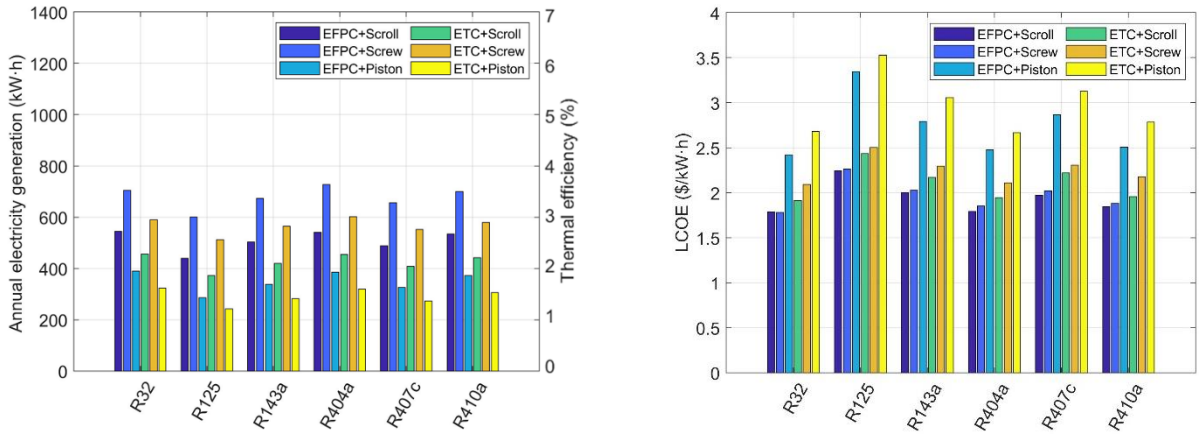

(a) (b)

Figure 15. (a) Annual electricity generation; and (b) corresponding LCOE for solar-ORC systems based on TNORCs. Ten investigated fluids are displayed in order of increasing critical temperature and cycle parameters optimised to achieve maximum annual electricity generation. Results were obtained for a solar-array area of 15 m^2 and annual hourly weather data in London, UK.

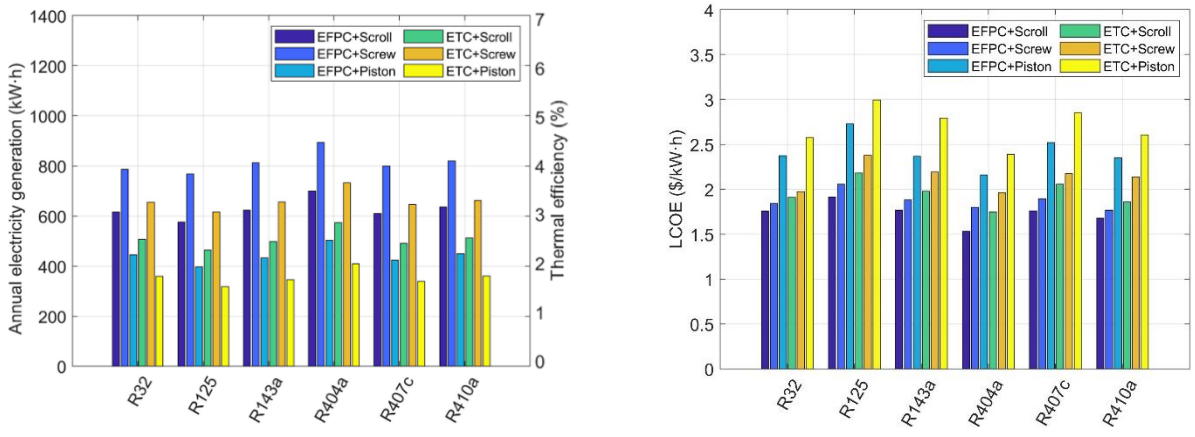

(a) (b)

Figure 16. (a) Annual electricity generation; and (b) corresponding LCOE for solar-ORC systems based on TRORCs. Ten investigated fluids are displayed in order of increasing critical temperature and cycle parameters optimised to achieve maximum annual electricity generation. Results were obtained for a solar-array area of 15 m^2 and annual hourly weather data in London, UK.

3.4. Annual off-design operation analysis

In the previous section, the design and operating conditions of the solar field and ORC system were optimised so as to maximise annual electricity generation, by examining a series of ORC configurations, component types and working fluids. While an (hourly) time-varying solar irradiance profile was used, the ORC system was only operated either ‘on’ at design/full-load conditions or switched ‘off’; the latter being initiated when there was not enough HTF in the hot storage tank available to allow the ORC system to operate continuously for at least 1 hour. In this section, a few optimal solar-ORC systems are selected, and the on/off operation of the power cycle is relaxed to

allow off-design ORC system operation (down to 50% load). Specifically, the system can operate when the HTF mass in the hot tank enables at least 1-hour operation at 50% load, and the actual operating load (HTF flow rate to the ORC system) is determined by the HTF mass in the hot tank. This operating strategy extends the operating hours of the ORC system, avoids frequent start-ups and shut-downs, and can also lead to performance benefits. The aim here is to identify the configuration and off-design operating points (temperatures, flow rates, pressures, etc.) that maximise annual electricity generation when controlled in manner that allows the ORC system to operate off-design. For this purpose, we firstly pre-select 9 system combinations based on their annual power generation potential in **Section 3.3**, and then use these to evaluate performance with off-design operation. The part-load performance of the expanders is considered explicitly in this analysis, and heat losses to the ambient are also accounted for. Detailed thermodynamic along with economic performance results are presented.

From the configurations examined in **Section 3.3**, the SRORC and EFPCs are selected because they outperform other candidates of the same category, with R1234ze, R152a and isobutane chosen because of their excellent thermoeconomic performance in SRORCs. For the three selected fluids, all expander types are considered, thus leading to nine combinations further investigated in this section.

Figure 17 shows results, generated following the approach explained in **Section 3.3**, of cost breakdowns for the selected combinations and payback times. Notably, the systems with screw expander have the highest investment cost (~$12,000) due to the relatively high expander cost, while systems with scroll and piston expanders have a total cost around $9,000. The system with piston expander and isobutane as the working fluid has the shortest payback time, yet still high, of 69 years. The long payback time is mainly caused by the low annual operating hours and the high cost of components. Development of small-scale expanders and solar collector technology would be helpful to reduce the system investment cost, thus leading to a short payback period. Furthermore, **Figure 18** which also relates to the approach in **Section 3.3**, shows that the annual operating hours of the selected systems are in the range 1,050-1,250, the net power output ranges from 0.8 kW to 1 kW, and the annual electricity generation could cover 35-40% of the electricity usage of a typical UK household [66].

In the annual operation analysis, it should be noted that: (i) actual hourly weather data throughout the whole year is used; (ii) the heat loss from the tank to the ambient is taken into account; and (iii) the minimum continuous operating time is still 1 hour but the power cycle is allowed to operate in part load (50%-100% of the design load), which means the HTF mass flow rate that flows to the power cycle can be 50-100% of the design value. The optimisation will then aim to identify those ORC operating conditions to maximise annual electricity generation, given the reduced HTF mass flow rate.

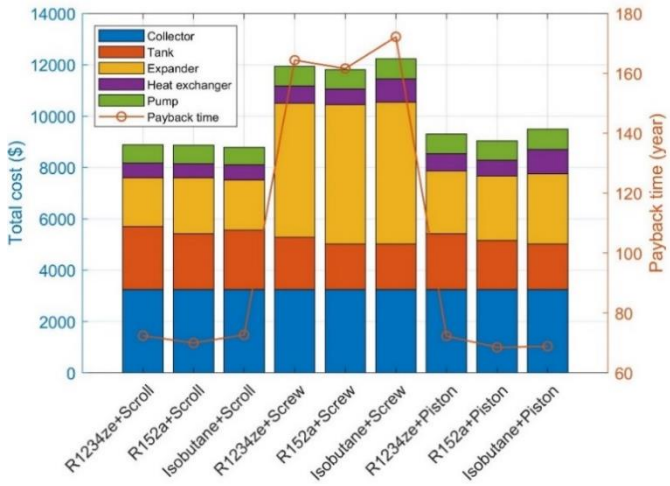

Figure 17. Cost breakdown of components in selected solar-ORC systems based on SRORCs and EFPCs. Results were obtained for a solar-array area of 15 m^2 and annual hourly weather data in London, UK, , following the approach outlined in **Section 3.3**.

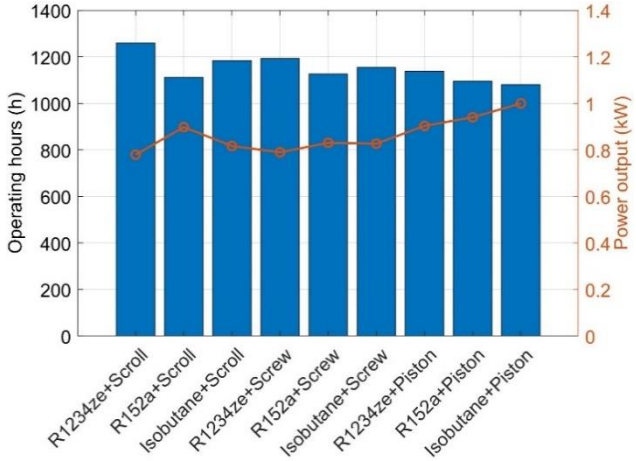

Figure 18. Annual operating hours and net power output of selected solar-ORC systems based on SRORCs and EFPCs. Results were obtained for a solar-array area of 15 m^2 and annual hourly weather data in London, UK, following the approach outlined in **Section 3.3**.

Figure 19 shows that, with off-design operation, the piston expander is still the most favoured, whilst the screw expander has the worst performance. The use of isobutane and a piston expander results in the highest annual electricity (1,100 kW ħ) and overall system efficiency (5.5%). **Figure 20** shows the operating hours breakdown of the solar power system utilising the SRORC, the EFPCs, the piston expander, and isobutane. The solar power system can run for 1,360 hours per year, which is 20% higher than the design condition, and the breakdown of operating hours by part-load condition 90-100% load, 80-90% load, 70-80% load, 60-70% load, and 50-60% load, are 246, 245, 209, 152, and 509, respectively. **Figure 21 and 22** show the solar irradiance and the operating details of a typical summer day and a typical winter day. On the summer day, the solar power system can continuously work for eight hours, with six hours' full load operation (~1 kW) from 12:00 to 18:00. On the winter day, the system can only work for two hours at part load conditions (0.68 kW and 0.55 kW).

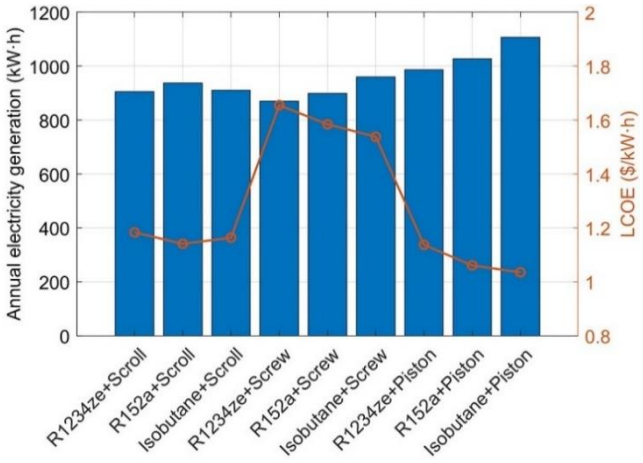

Figure 19. Annual electricity generation and LCOE of solar-ORC systems based on SRORCs and EFPCs. Results were obtained for a solar-array area of 15 m^2 and annual hourly weather data in London, UK.

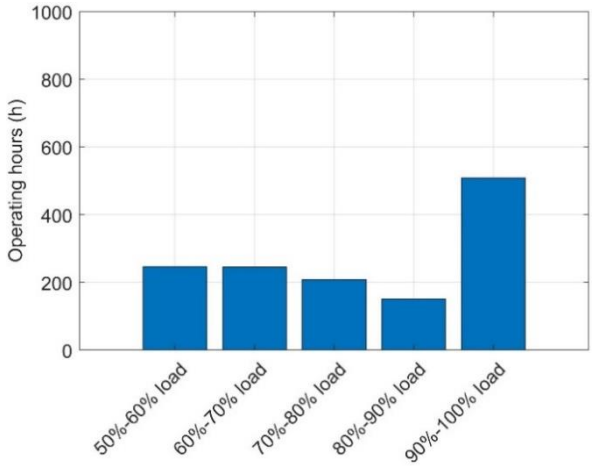

Figure 20. Annual operating hours breakdown in terms of load ranges for a solar-ORC system based on a SRORC, EFPCs, a piston expander and isobutane as the working fluid. Results were obtained for a solar-array area of 15 m^2 and annual hourly weather data in London, UK.

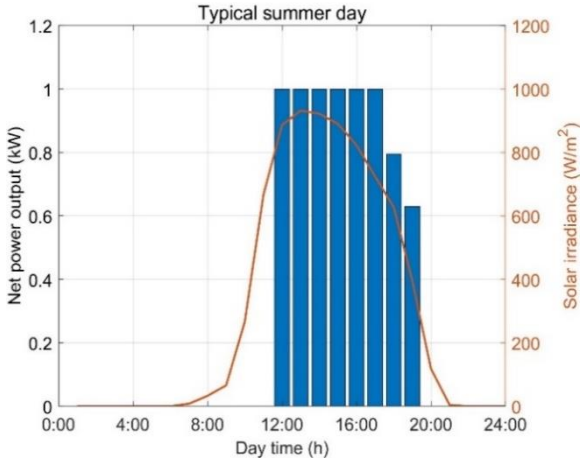

Figure 21. Solar irradiance and operating details on a typical summer day for a solar-ORC system based on a SRORC, EFPCs, a piston expander, and isobutane as the working fluid. Results were obtained for a solar-array area of 15 m^2 and annual hourly weather data in London, UK.

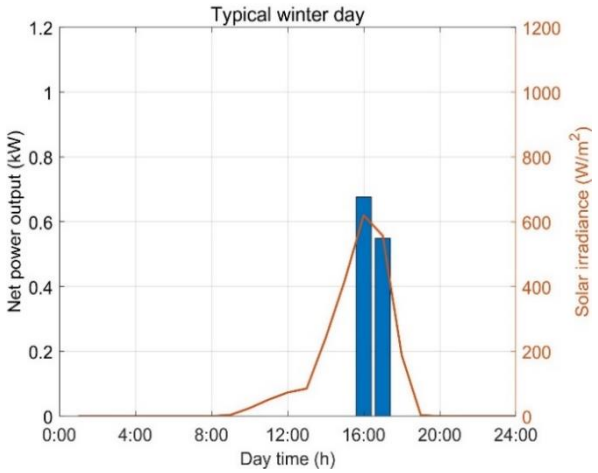

Figure 22. Solar irradiance and operating details on a typical summer day for a solar-ORC system based on a SRORC, EFPCs, a piston expander, and isobutane as the working fluid. Results were obtained for a solar-array area of 15 m^2 and annual hourly weather data in London, UK.

3.5 Generalised multi-region and climate analysis

The investigations of the various solar-ORC system above are all based on the UK climate, where such systems have relatively long payback times because of the moderate solar resource in the UK (~1,450 sunshine hours, 920 W/m^2 ħ). In this section, a wide range of annual sunshine hours (1,200-4,000 h) and average solar irradiance (800-1100 W/m^2 ħ) representing different regions/climates are considered. The annual electricity generation for each system is calculated by running steady-state simulations using the annually-averaged solar irradiance as an input, accounting for both direct and diffuse irradiance components, and then multiplying the generated electricity with the sunshine hours. The average annual solar irradiance in London is around 1,400 kW/m^2, while it can reach 3,000 kW/m^2 in the US and China and even >4,000 kW/m^2 in Chile [67].

As in **Section 3.3**, the tank storage temperatures and cycle parameters are optimised to achieve maximum power generation, different isentropic efficiencies corresponding to the expander type are considered, no heat loss are assumed and the ORC system is always operated at full load if there is enough HTF to run the system for at least 1 hour. Importantly, it is found that the optimal solar-ORC system remains the same the different solar conditions being considered here. For a fixed solar-array area of 15 m^2, the system based on the SRORC, EFPCs, a piston expander, and isobutane as the working fluid provides the maximum annual electricity generation, so this system is selected in this section.

Figure 23 shows that the annual electricity generation of the solar-ORC system increases with the sunshine hours and average solar irradiance of sunshine hours. The solar-ORC system can produce ~72 kW ħ/m^2 of solar collection areas in the London climate, and the same system can produce >200 kW ħ/m^2 annually (increase of ~180%) in those areas with long sunshine hours and intensive irradiation, for instance, Chile. As seen from **Figure 24**, the LCOE of the presented solar-ORC system has lower LCOE (as low as <0.35 $/kW ħ) in areas with longer sunshine hours and

higher solar irradiance. **Figure 25** shows the payback time of the solar-ORC system in different solar conditions. The system in the London climate has a payback time of >60 years, while the system in those areas with long sunshine hours and intensive irradiation (such as in Chile) can get the investment cost back in <16 years. The relatively long payback time of the presented solar-ORC system is mainly due to the high costs of the components, especially the collectors and expanders which have the potential for cost-reduction with the technology development in the near future.

The ranges of sunshine hours and solar irradiance investigated in this work cover solar conditions relevant to a wide diversity of global regions. The methods and results presented in this paper, therefore, can be useful for preliminary assessments of the thermoeconomic potential small-scale solar-ORC systems across a range of local climate conditions. Once the annual sunshine hours and average solar irradiance are known for a specific location, the technoeconomic viability and potential of installing small-scale solar-ORC power systems at that location can be assessed using the performance maps in **Figure 23-25**. The performance maps can be further extended and improved if additional options, i.e., solar collectors, cycle configurations, expander types and working fluids, are to be considered. Extended system scales/sizes as well as applications and functions (electricity generation or cogeneration) remain of interest for further investigations.

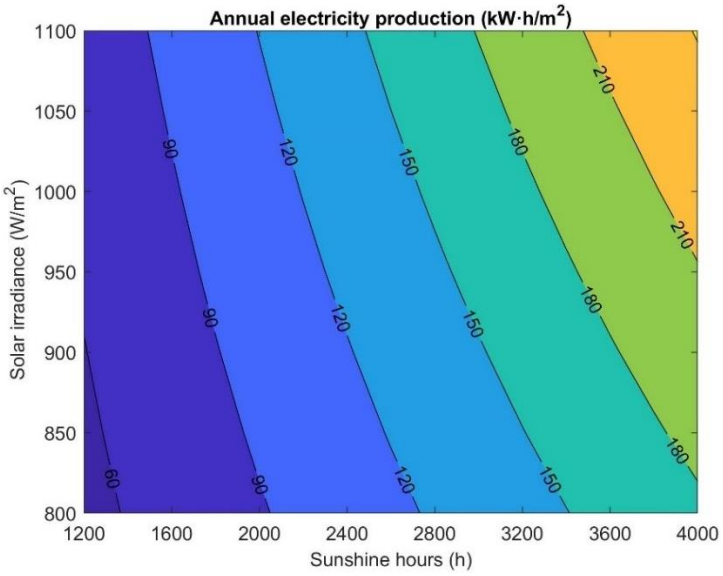

Figure 23. Annual electricity generation of solar-ORC systems based on SRORCs, with a fixed EFPCs solar-array area of 15 m^2, piston expanders, and isobutane as the working fluid, which provide the maximum annual electricity generation among all designs with respect to annual sunshine hours and average solar irradiance. The sunshine hours range from 1,200 to 4,000 h and the average solar irradiance from 800 to 1,100 W/m^2 ħ, which represents the solar conditions found of most global regions. The solar irradiance includes beam and diffuse components.

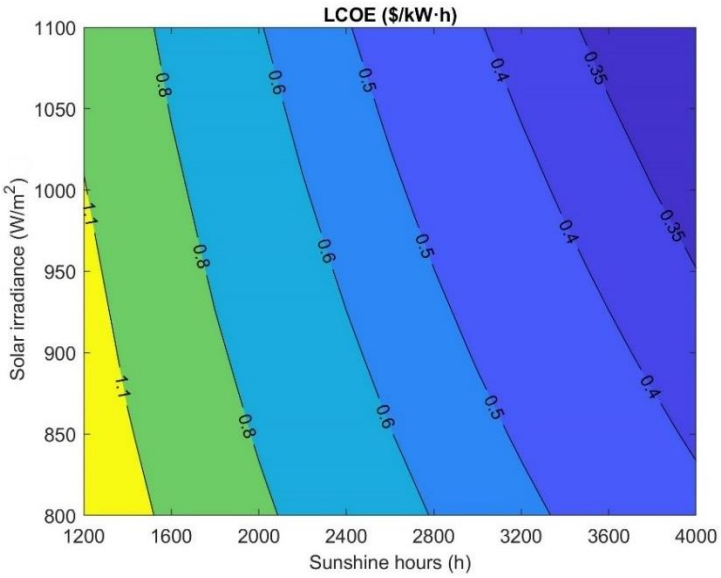

Figure 24. LCOE of solar-ORC systems based on SRORCs, with a fixed EFPCs solar-array area of 15 m^2, piston expanders, and isobutane as the working fluid, which provide the maximum annual electricity generation among all designs with respect to annual sunshine hours and average solar irradiance. The sunshine hours range from 1,200 to 4,000 h and the average solar irradiance from 800 to 1,100 W/m^2 ħ, which represents the solar conditions found of most global regions. The solar irradiance includes beam and diffuse components.

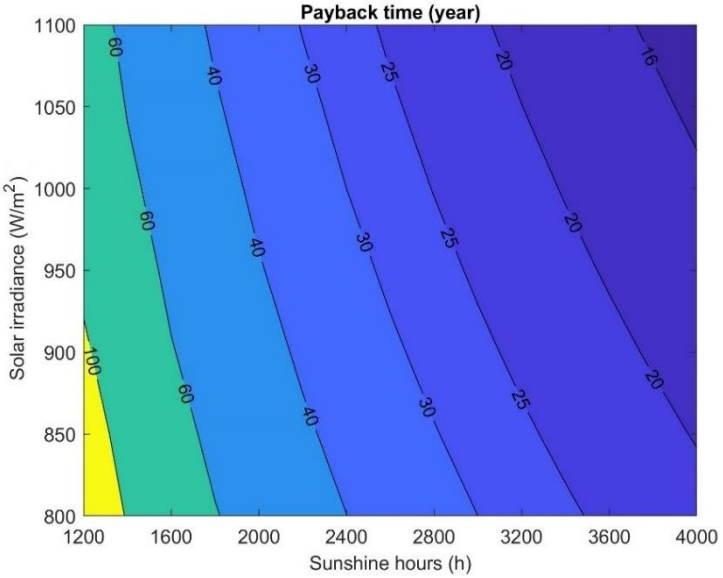

Figure 25. Payback time of solar-ORC systems based on SRORCs, with a fixed EFPCs solar-array area of 15 m^2, piston expanders, and isobutane as the working fluid, which provide the maximum annual electricity generation among all designs with respect to annual sunshine hours and average solar irradiance. The sunshine hours range from 1,200 to 4,000 h and the average solar irradiance from 800 to 1,100 W/m^2 ħ, which represents the solar conditions found of most global regions. The solar irradiance includes beam and diffuse components.

4. Conclusions

In this paper, a variety of domestic solar-ORC systems based on a fixed solar-array area of 15 m^2 and two-tank thermal-energy storage were studied based on both technical and economic considerations. Optimal systems were identified that delivered maximum electricity generation over an annual period, along with key corresponding economic parameters (LCOE, payback time). The investigations covered six power cycle configurations, three collector types, three expander types, and sixteen working fluids, specifically: (i) flat-plate, evacuated-tube and evacuated flat-plate collectors; (ii) (basic/recuperative, partial/full evaporating and subcritical/transcritical power cycle configurations; (iii) scroll, screw, and piston expanders; and (iv) a selection of working fluids considered suitable for this application. Two operating strategies were considered: (i) the ORC system was only operated at a full load with periodic start-up/shut-downs in response to the varying thermal-energy availability from the storage tanks; and (ii) off-design ORC system operation was allowed down to 50% load, which extended the operating hours of the ORC system, avoided frequent start-ups and shut-downs, and lead to small performance benefits. Although the study initially focused on London, UK, taken as representative temperate climate with modest temperature changes, mild winters and moderate summers, it was extended considered a wider range of climates. This work goes beyond previous research by undertaking, for the first time, a comprehensive comparison of domestic-scale solar-ORC system variants based on their thermoeconomic performance when operating under different time-varying solar conditions, using a unified modelling framework that promotes more confident comparisons between the systems.

The trade-off between optimising the performance of the solar field and the performance of the power cycle was first investigated, with results showing that lower tank storage temperatures lead to higher collector thermal efficiencies, whilst higher temperatures allow higher power cycle thermal efficiencies, and vice versa, which highlighted the importance of balancing this trade-off.

System optimisation was then formulated to maximise the annual electricity generation of solar-ORC systems in London when operated only at full-load and to pre-screen best-performing designs. Solar-ORC systems based on subcritical, recuperated cycles (SRORCs) and with evacuated flat-plate collectors (EFPCs) achieved the best thermodynamic and economic performance relative to other systems, delivering 1,080 kW ħ (with a corresponding thermal efficiency of 5.4%) of electricity per year at a LCOE down to ~1 $/kW ħ. The highest overall system thermal efficiency was 10-50% higher and corresponding LCOE 5-40% lower than other systems investigated in this work. Furthermore, all three expanders showed good thermodynamic performance, but scroll and piston expanders also showed good economic performance, and three working fluids with relatively low critical temperatures (R1234yf, R152a, and isobutane) were identified as enabling best performance in this application.

A set of pre-screened designs were selected for further investigation, in annual simulations that allowed off-design operation. Systems based on the SRORC, EFPCs, a piston expander and isobutane as the working fluid provided the highest annual electricity generation of 1,100 kW ħ/year with an overall thermal efficiency of 5.5%, which was 5-30% higher than the other selected designs, and the corresponding LCOE was ~1 $/kW ħ, which was 3-35% lower than the other selected designs. Detailed

operation of typical summer and winter days was performed, with results indicating that, by allowing the system to be operated at part load (50%-100% of the design load), the operating hours of the system can be improved by more than 20% whilst maintaining the annual electricity generation potential.

When considering a wider variety solar conditions (irradiance from 800 to 1,100 W/m^2 ħ, sunshine hours from 1,200 to 4,000 h), the optimal solar-ORC systems that achieves the maximum annual electricity generation remains unchanged, i.e., a system utilising a SRORC, EFPCs, a piston expander, and isobutane as the working fluid. However, LCOEs <0.35 $/kW ħ and payback times <16 years can be achieved in solar-rich regions (sunshine hours >3,800 h, solar irradiance >1,000 W/m^2 ħ).

In closing, it is noted that solar-ORC technology offers advantages (with respect to alternatives based on PV) in applications where the co-/poly-generation of heating and/or cooling, and where storage is required as they can benefit from low-cost thermal energy storage. The results presented here highlight the need to optimally integrate the solar field and power cycle in domestic solar-ORC systems, and provide valuable guidance on selecting appropriate configurations, components, and working fluids for such systems. Domestic solar-ORC systems are technically feasible, and likely to be increasingly commercially viable with the development of high-performance and low-cost components such as collectors and expanders, especially in regions with an abundant solar resource.

Acknowledgements

This work was supported by the UK Engineering and Physical Sciences Research Council (EPSRC) [grant numbers EP/P004709/1, EP/R045518/1], and the China Scholarship Council (CSC) for a Joint-PhD scholarship [grant number 201906280377] that supported Yaxiong Wang's visit at Imperial College London. This work was also supported by an Institutional Links grant, ID 352350650, under the Newton-Mosharafa Fund partnership. The grant is funded by the UK Department for Business, Energy and Industrial Strategy and the Science and Technology Development Fund, and delivered by the British Council. For further information, please visit www.newtonfund.ac.uk. Data supporting this publication can be obtained on request from cep-lab@imperial.ac.uk.

References

[1] Li FF, Qiu J. Multi-objective optimization for integrated hydro-photovoltaic power system. Appl Energy 2016;167:377–84.

[2] Aktas A, Erhan K, Özdemir S, Özdemir E. Dynamic energy management for photovoltaic power system including hybrid energy storage in smart grid applications. Energy 2018;162:72–82.

[3] Akinyele DO, Rayudu RK. Comprehensive techno-economic and environmental impact study of a localised photovoltaic power system (PPS) for off-grid communities. Energy Convers Manag 2016;124:266–79.

[4] Morrone P, Algieri A, Castiglione T. Hybridisation of biomass and concentrated solar power systems in transcritical organic Rankine cycles: A micro combined heat and power application. Energy Convers Manag 2019;180:757–68.

[5] He YL, Wang K, Qiu Y, Du BC, Liang Q, Du S. Review of the solar flux distribution in concentrated solar power: Non-uniform features, challenges, and solutions. Appl Therm Eng 2019;149:448–74.

[6] Stein WH, Buck R. Advanced power cycles for concentrated solar power. Sol Energy 2017;152:91–105.

[7] Lorestani A, Ardehali MM. Optimization of autonomous combined heat and power system including PVT, WT, storages, and electric heat utilizing novel evolutionary particle swarm optimization algorithm. Renew Energy 2018;119:490–503.

[8] Herrando M, Ramos A, Zabalza I. Cost competitiveness of a novel PVT-based solar combined heating and power system: Influence of economic parameters and financial incentives. Energy Convers Manag 2018;166:758–70.

[9] Wang K, Herrando M, Pantaleo AM, Markides CN. Technoeconomic assessments of hybrid photovoltaic-thermal vs. conventional solar-energy systems: Case studies in heat and power provision to sports centres. Appl Energy 2019;254:113657.

[10] Freeman J, Hellgardt K, Markides CN. An assessment of solar-powered organic Rankine cycle systems for combined heating and power in UK domestic applications. Appl Energy 2015;138:605–20.

[11] Freeman J, Hellgardt K, Markides CN. Working fluid selection and electrical performance optimisation of a domestic solar-ORC combined heat and power system for year-round operation in the UK. Appl Energy 2017;186:291–303.

[12] Freeman J, Guarracino I, Kalogirou SA, Markides CN. A small-scale solar organic Rankine cycle combined heat and power system with integrated thermal energy storage. Appl Therm Eng 2017;127:1543–54.

[13] Ramos A, Chatzopoulou MA, Freeman J, Markides CN. Optimisation of a high-efficiency solar-driven organic Rankine cycle for applications in the built environment. Appl Energy 2018;228:755–65.

[14] Sonsaree S, Asaoka T, Jiajitsawat S, Aguirre H, Tanaka K. A small-scale solar Organic Rankine Cycle power plant in Thailand: Three types of non-concentrating solar collectors. Sol Energy 2018;162:541–60.

[15] Helvaci HU, Khan ZA. Thermodynamic modelling and analysis of a solar organic Rankine cycle employing thermofluids. Energy Convers Manag 2017;138:493–510.

[16] Wang R, Jiang L, Ma Z, Gonzalez-Diaz A, Wang Y, Roskilly A. Comparative Analysis of Small-Scale Organic Rankine Cycle Systems for Solar Energy Utilisation. Energies 2019;12:829.

[17] Roumpedakis TC, Loumpardis G, Monokrousou E, Braimakis K, Charalampidis A, Karellas S. Exergetic and economic analysis of a solar driven small scale ORC. Renew Energy 2020;157:1008–24.

[18] Yari M, Mehr AS, Zare V, Mahmoudi SMS, Rosen MA. Exergoeconomic comparison of TLC (trilateral Rankine cycle), ORC (organic Rankine cycle) and Kalina cycle using a low grade heat source. Energy 2015;83:712–22.

[19] Li Z, Lu Y, Huang Y, Qian G, Chen F, Yu X, et al. Comparison study of Trilateral Rankine Cycle, Organic Flash Cycle and basic Organic Rankine Cycle for low grade heat recovery. Energy Procedia 2017;142:1441–7.

[20] Zhou Y, Zhang F, Yu L. Performance analysis of the partial evaporating organic Rankine cycle (PEORC) using zeotropic mixtures. Energy Convers Manag 2016;129:89–99.

[21] Lecompte S, Chatzopoulou MA, Markides CN, De Paepe M. Off-design comparison of subcritical and partial evaporating ORCs in quasi-steady state annual simulations. Energy Procedia 2019;158:2064–9.

[22] Lecompte S, Huisseune H, van den Broek M, De Paepe M. Methodical thermodynamic analysis and regression models of organic Rankine cycle architectures for waste heat recovery. Energy 2015;87:60–76.

[23] Zeynali A, Akbari A, Khalilian M. Investigation of the performance of modified organic Rankine cycles (ORCs) and modified trilateral flash cycles (TFCs) assisted by a solar pond. Sol Energy 2019;182:361–81.

[24] Oyewunmi OA, Lecompte S, De Paepe M, Markides CN. Thermoeconomic analysis of recuperative sub- and transcritical organic Rankine cycle systems. Energy Procedia 2017;129:58–65.

[25] Wu Y, Guo Z, Lei B, Shen L, Zhi R. Internal volume ratio optimization and performance analysis for single-screw expander in small-scale middle temperature ORC system. Energy 2019;186:115799.

[26] Ziviani D, James NA, Accorsi FA, Braun JE, Groll EA. Experimental and numerical analyses of a 5 kWe oil-free open-drive scroll expander for small-scale organic Rankine cycle (ORC) applications. Appl Energy 2018;230:1140–56.

[27] Bianchi M, Branchini L, Casari N, De Pascale A, Melino F, Ottaviano S, et al. Experimental analysis of a micro-ORC driven by piston expander for low-grade heat recovery. Appl Therm Eng 2019;148:1278–91.

[28] Dumont O, Parthoens A, Dickes R, Lemort V. Experimental investigation and optimal performance assessment of four volumetric expanders (scroll, screw, piston and roots) tested in a small-scale organic Rankine cycle system. Energy 2018;165:1119–27.

[29] Guillaume L, Lemort V. Comparison of different ORC typologies for heavy-duty trucks by means of a thermo-economic optimization. Energy 2019;182:706–28.

[30] Kanno H, Shikazono N. Modeling study on two-phase adiabatic expansion in a reciprocating expander. Int J Heat Mass Transf 2017;104:142–8.

[31] Öhman H, Lundqvist P. Experimental investigation of a Lysholm Turbine operating with superheated, saturated and 2-phase inlet conditions. Appl Therm Eng 2013;50:1211–8.

[32] Kosmadakis G, Manolakos D, Papadakis G. Experimental investigation of a lowerature organic Rankine cycle (ORC) engine under variable heat input operating at both subcritical and supercritical conditions. Appl Therm Eng 2016;92:1–7.

[33] Hsieh JC, Fu BR, Wang TW, Cheng Y, Lee YR, Chang JC. Design and preliminary results of a 20-kW transcritical organic Rankine cycle with a screw expander for low-grade waste heat recovery. Appl Therm Eng 2017;110:1120–7.

[34] Li M, Ma Y, Guan H, Li L. Development and Experimental Study of CO 2 Expander in CO 2 Supercritical Refrigeration Cycles. Int J Green Energy 2004;1:89–99.

[35] Therminol VP-1 Heat Transfer Fluid. https://www.therminol.com/product/71093459 (accessed August 5, 2020).

[36] Flat plate collectors PremiumPlus. https://www.solarbayer.com/Flat-plate-collector-

PremiumPlus.html (accessed May 23, 2020).
[37] THERMOMAX Technical Design Guide. http://www.kingspansolar.ie/pdf/thermomaxdesignguide.pdf (accessed May 23, 2020).
[38] MT-Power Product datasheet. https://www.tvpsolar.com/products.html (accessed May 23, 2020).
[39] Petrollese M, Cocco D. Robust optimization for the preliminary design of solar organic Rankine cycle (ORC) systems. Energy Convers Manag 2019;184:338–49.
[40] Bao J, Zhao L. A review of working fluid and expander selections for organic Rankine cycle. Renew Sustain Energy Rev 2013;24:325–42.
[41] Imran M, Usman M, Park BS, Lee DH. Volumetric expanders for low grade heat and waste heat recovery applications. Renew Sustain Energy Rev 2016;57:1090–109.
[42] Astolfi M. Techno-economic Optimization of Low Temperature CSP Systems Based on ORC with Screw Expanders. Energy Procedia 2015;69:1100–12.
[43] Unamba CK, Sapin P, Li X, Song J, Wang K, Shu G, et al. applied sciences Operational Optimisation of a Non-Recuperative 1-kWe Organic Rankine Cycle (ORC) Engine Prototype. Energies 2019;9:3024.
[44] Lemort V, Declaye S, Quoilin S. Experimental characterization of a hermeti scroll expander for use in a micro-scale Rankine cycle. Proc Inst Mech Eng Part A J Power Energy 2012;226:126–36.
[45] Simpson M, Rotolo G, Sapin P, De Palma P, White AJ, Markides CN. Thermodynamic performance maps of reciprocating-piston expanders for operation at off-design and part-load conditions. 13th Int. Conf. Heat Transf. Fluid Mech. Thermodyn., Portorož: HEFAT; 2017.
[46] Sapin P, Simpson M, White AJ, Markides CN. Lumped Dynamic Analysis and Design of a High-Performance Reciprocating-Piston Expander. 30th Int. Conf. Effic. Cost, Optimisation, Simul. Environ. Impact Energy Syst., ECOS; 2017.
[47] Chatzopoulou MA, Simpson M, Sapin P, Markides CN. Off-design optimisation of organic Rankine cycle (ORC) engines with piston expanders for medium-scale combined heat and power applications. Appl Energy 2019;238:1211–36.
[48] Chatzopoulou MA, Lecompte S, Paepe M De, Markides CN. Off-design optimisation of organic Rankine cycle (ORC) engines with different heat exchangers and volumetric expanders in waste heat recovery applications. Appl Energy 2019;253:113442.
[49] Alshammari F, Karvountzis-Kontakiotis A, Pesyridis A, Usman M. Expander technologies for automotive engine organic rankine cycle applications. Energies 2018;11:1905.
[50] Quoilin S, Declaye S, Tchanche BF, Lemort V. Thermo-economic optimization of waste heat recovery Organic Rankine Cycles. Appl Therm Eng 2011;31:2885–93.
[51] Patil VR, Biradar VI, Shreyas R, Garg P, Orosz MS, Thirumalai NC. Techno-economic comparison of solar organic Rankine cycle (ORC) and photovoltaic (PV) systems with energy storage. Renew Energy 2017;113:1250–60.
[52] Herrando M, Ramos A, Freeman J, Zabalza I, Markides CN. Technoeconomic modelling and optimisation of solar combined heat and power systems based on flat-box PVT collectors for domestic applications. Energy Convers Manag 2018;175:67–85.
[53] Weather Data | EnergyPlus. https://energyplus.net/weather (accessed September 7, 2020).
[54] Braimakis K, Karellas S. Energetic optimization of regenerative Organic Rankine Cycle

(ORC) configurations. Energy Convers Manag 2018;159:353–70.

[55] Shahverdi K, Loni R, Ghobadian B, Monem MJ, Gohari S, Marofi S, et al. Energy harvesting using solar ORC system and Archimedes Screw Turbine (AST) combination with different refrigerant working fluids. Energy Convers Manag 2019;187:205–20.

[56] Song J, Wang Y, Wang K, Wang J, Markides CN. Combined supercritical CO_2 (SCO_2) cycle and organic Rankine cycle (ORC) system for hybrid solar and geothermal power generation: Thermoeconomic assessment of various configurations. Renew Energy 2021;174:1020–35.

[57] Lemmon EW, Huber ML, McLinden MO. NIST reference fluid thermodynamic and transport properties–REFPROP 2002.

[58] Wang H, Peterson RB, Herron T. Experimental performance of a compliant scroll expander for an organic Rankine cycle. Proc Inst Mech Eng Part A J Power Energy 2009;223:863–72.

[59] Ayachi F, Ksayer EB, Neveu P, Zoughaib A. Experimental investigation and modeling of a hermetic scroll expander. Appl Energy 2016;181:256–67.

[60] Quoilin S, Lemort V, Lebrun J. Experimental study and modeling of an Organic Rankine Cycle using scroll expander. Appl Energy 2010;87:1260–8.

[61] Lei B, Wang W, Wu YT, Ma CF, Wang JF, Zhang L, et al. Development and experimental study on a single screw expander integrated into an Organic Rankine Cycle. Energy 2016;116:43–52.

[62] Ziviani D, Gusev S, Lecompte S, Groll EA, Braun JE, Horton WT, et al. Characterizing the performance of a single-screw expander in a small-scale organic Rankine cycle for waste heat recovery. Appl Energy 2016;181:155–70.

[63] Avadhanula VK, Lin C Sen. Empirical models for a screw expander based on experimental data from organic rankine cycle system testing. J Eng Gas Turbines Power 2014;136.

[64] Hsu S-W, Chiang H-W, Yen C-W. Experimental Investigation of the Performance of a Hermetic Screw-Expander Organic Rankine Cycle. Energies 2014;7:6172–85.

[65] Oudkerk J-F, Dickes R, Dumont O, Lemort V. Experimental performance of a piston expander in a small-scale organic Rankine cycle. IOP Conf Ser Mater Sci Eng 2015;90:12066.

[66] The Average Gas & Electricity Usage in the UK - Smarter Business. https://smarterbusiness.co.uk/blogs/average-gas-electricity-usage-uk/ (accessed September 9, 2020).

[67] Global Solar Atlas. https://globalsolaratlas.info/map (accessed January 22, 2021).

[68] Garc á-Cascales JR, Vera-Garc á F, Corber án-Salvador JM, Gonz álvez-Maci á J. Assessment of boiling and condensation heat transfer correlations in the modelling of plate heat exchangers. Int J Refrig 2007;30:1029–41.

[69] Han DH, Lee KJ, Kim YH. Experiments on the characteristics of evaporation of R410A in brazed plate heat exchangers with different geometric configurations. Appl Therm Eng 2003;23:1209–25.

[70] Han D-H, Lee K-J, Kim Y-H. The Characteristics of Condensation in Brazed Plate Heat Exchangers with Different Chevron Angles. J Korean Phys Soc 2003;43:66–73.

Appendix A. Plate heat exchanger model

For plate heat exchangers, heat transfer coefficients and pressure drops for both the HTF and the working fluid are calculated from the following equations.

A.1. Single-phase region

The heat transfer coefficients of the HTF and the working fluid in single-phase heat transfer are described using the same equations by Chisholm and Waniarchi [68]:

$$\alpha = Nu\frac{\lambda_{\mathrm{wf}}}{D_{\mathrm{h}}}, \tag{A.1}$$

where the Nusselt number *Nu* can be expressed as:

$$Nu = 0.724\left(6\beta/\pi\right)^{0.646}\,\mathrm{Re}^{0.583}\,\mathrm{Pr}^{1/3}, \tag{A.2}$$

where the Reynolds number *Re* is calculated from:

$$\mathrm{Re} = \frac{\rho u D_{\mathrm{h}}}{\nu}, \tag{A.3}$$

where the fluid velocity can be calculated from:

$$u = \frac{\dot{m}}{\rho S_{\mathrm{p}}}. \tag{A.4}$$

The pressure drop of both the HTF and the working fluid is estimated using the same equations proposed by Kind and Martin [48]:

$$P_{\mathrm{loss}} = 4 f_{\mathrm{p}}\frac{L_{\mathrm{p}}}{D_{\mathrm{h}}}\frac{G_{\mathrm{p}}^2}{2\rho}, \tag{A.5}$$

$$\frac{1}{\sqrt{f_{\mathrm{p}}}} = \frac{\cos\beta}{\left(0.18\tan\beta + 0.36\sin\beta + f_0/\cos\beta\right)^{0.5}} + \frac{1-\cos\beta}{\sqrt{3.8 f_1}}, \tag{A.6}$$

$$\begin{aligned} &f_0 = \frac{64}{\mathrm{Re}},\ f_1 = \frac{597}{\mathrm{Re}} + 3.85, && \text{for } \mathrm{Re} < 2000, \\ &f_0 = \left(1.8\log_{10}\mathrm{Re} - 1.5\right)^{-2},\ f_1 = \frac{39}{\mathrm{Re}^{0.289}}, && \text{for } \mathrm{Re} \geq 2000. \end{aligned} \tag{A.7}$$

A.2. Evaporation process

The heat transfer coefficient of the working fluid during the evaporation process is estimated by the correlation proposed by Han [69]:

$$\alpha_{\mathrm{wf}} = c_1\frac{\lambda_{\mathrm{wf,l}}}{D_{\mathrm{h}}}\mathrm{Re}_{\mathrm{wf,eq}}^{c_2}\,Bo_{\mathrm{eq}}^{0.3}\,\mathrm{Pr}_{\mathrm{wf,l}}^{0.4}, \tag{A.8}$$

$$\mathrm{Re}_{\mathrm{wf,eq}} = \frac{G_{\mathrm{wf,eq}} D_{\mathrm{h}}}{\mu_{\mathrm{wf,l}}}, \tag{A.9}$$

$$G_{\mathrm{wf,eq}} = G_{\mathrm{wf,p}} \left[1 - x + x \left(\frac{\rho_{\mathrm{wf,l}}}{\rho_{\mathrm{wf,v}}} \right)^{0.5} \right], \tag{A.10}$$

$$Bo_{\mathrm{wf,eq}} = \frac{\dot{q}_{\mathrm{wf}}}{G_{\mathrm{wf,eq}} h_{\mathrm{lg}}}, \tag{A.11}$$

$$\dot{q}_{\mathrm{wf,eq}} = \frac{\dot{Q}_{\mathrm{ev}}}{A_{\mathrm{ev}}}, \tag{A.12}$$

$$c_1 = 2.81 \left(\frac{z}{D_h} \right)^{-0.041} \beta^{-2.83}, \tag{A.13}$$

$$c_2 = 0.746 \left(\frac{z}{D_h} \right)^{-0.082} \beta^{0.61}. \tag{A.14}$$

The pressure drop of the working fluid in the evaporation process is calculated using the correlations developed by Han [69]:

$$P_{\mathrm{loss,wf}} = 4 f_{\mathrm{p,wf}} \frac{L_{\mathrm{p}}}{D_{\mathrm{h}}} \frac{G_{\mathrm{wf,eq}}^2}{2 \rho_{\mathrm{wf,l}}}, \tag{A.15}$$

$$f_{\mathrm{p}} = c_3 \, \mathrm{Re}_{\mathrm{wf,eq}}^{c_4}, \tag{A.16}$$

$$c_3 = 64710 \left(\frac{z}{D_{\mathrm{h}}} \right)^{-5.27} \left(\frac{\pi}{2} - \beta \right)^{-3.03}, \tag{A.17}$$

$$c_4 = -1.314 \left(\frac{z}{D_{\mathrm{h}}} \right)^{-0.62} \left(\frac{\pi}{2} - \beta \right)^{-0.47}. \tag{A.18}$$

A.3. Condensation process

During condensation, the correlations developed by Han [70] is applied and the heat transfer coefficient of the working fluid can be expressed as:

$$\alpha_{\mathrm{wf}} = c_5 \frac{\lambda_{\mathrm{wf,l}}}{D_{\mathrm{h}}} \mathrm{Re}_{\mathrm{wf,eq}}^{c_6} \, \mathrm{Pr}_{\mathrm{wf,l}}^{1/3}, \tag{A.19}$$

$$c_5 = 11.22 \left(\frac{z}{D_{\mathrm{h}}} \right)^{-2.83} \beta^{-4.5}, \tag{A.20}$$

$$c_6 = 0.35 \left(\frac{z}{D_{\mathrm{h}}} \right)^{0.23} \beta^{1.48}. \tag{A.21}$$

The pressure loss in condensation process is calculated using the Han correlations [70]:

$$P_{\text{loss,wf}} = 4 f_{\text{p,wf}} \frac{L_{\text{p}}}{D_{\text{h}}} \frac{G_{\text{wf,eq}}^2}{2\rho_{\text{wf,l}}}, \tag{A.22}$$

$$f_{\text{p}} = c_7 \, \text{Re}_{\text{wf,eq}}^{c_8}, \tag{A.23}$$

$$c_7 = 3521.1 \left(\frac{z}{D_{\text{h}}} \right)^{4.17} \beta^{-7.75}, \tag{A.24}$$

$$c_8 = -1.024 \left(\frac{z}{D_{\text{h}}} \right)^{0.0925} \beta^{-1.3}. \tag{A.25}$$